Uncovering the Transmembrane Protein 43 life cycle to provide insight into Arrhythmogenic Right Ventricular Cardiomyopathy

By © Hooman Sadighian

A Thesis submitted to the School of Graduate Studies in partial fulfillment of the requirements for the degree of

Master of Science in Medicine (Cardiovascular & Renal Sciences)

Division of BioMedical Sciences/Faculty of Medicine

Memorial University of Newfoundland

May 2021

St. John's, Newfoundland and Labrador

Foreword

I started my graduate education at MUN in September 2018. Dr. Dake Qi accepted me as a graduate student in Cardiovascular and Renal Sciences in the Faculty of Medicine. Eight months into my Master's degree, Dr. Qi accepted a position at the University of Manitoba. Although I found my graduate project stimulating, it was impossible for me to move to another city. Therefore, I stayed in St. John's at MUN and in September 2019, halfway through my MSc, Dr. Jessica Esseltine took over supervision of my graduate program.

My project with Dr. Esseltine was also well aligned to cardiovascular sciences, however, it was significantly different from the work I conducted with Dr. Qi. Therefore, my Master's thesis comprises two distinct projects, each comprising a year of my graduate studies. To that end, SGS and RGS have suggested that I prepare my thesis in the following format:

The main body of this thesis, including introduction, methods, results, and discussion, surrounds my research in Esseltine lab. The results of my first project with Dr. Qi can be found in appendix A.

Abstract

Arrhythmogenic Right Ventricular Cardiomyopathy (ARVC) is an inherited heart failure featuring sudden cardiac death. ARVC type 5 is caused by an autosomal dominant mutation in the transmembrane protein 43 (*TMEM43*) gene (c.1073C>T, p.S358L) widespread throughout the Newfoundland population. Although this mutation is known to cause ARVC type 5, very little is known about the wild type TMEM43 protein. In order to shed light on the basic functions of TMEM43, we used CRISPR-Cas9 to genetically ablate *TMEM43* in AD293 reference cells as well as human induced pluripotent stem cells (iPSCs). Cycloheximide pulse-chase experiments demonstrate that wild type TMEM43 has a relatively long half-life of more than 8 hours. Interestingly, while TMEM43 was localized to the nuclear envelope of AD293 cells, it was distributed primarily in large punctae throughout the cytoplasm of human iPSCs. Furthermore, TMEM43 may be more highly expressed in male (XY) iPSC-derived cardiomyocytes compared to female (XX) cells which could shed light on the sex differences observed in ARVC disease severity. These findings highlight some of the most basic features of the TMEM43 protein while future studies using the TMEM43 knockout cells may shed light on how *TMEM43* genetic mutation causes ARVC in Newfoundland.

Lay Summary

Arrhythmogenic Right Ventricular Cardiomyopathy (ARVC) is a devastating disease of the heart, which can lead to SCD in otherwise young, healthy people. ARVC can be caused by inherited genetic mutation passed down through families. Unfortunately, Newfoundland is home to one of the largest populations of ARVC patients in the world, caused by a mutation in a gene called transmembrane protein 43 (*TMEM43*). Children of affected individuals have a 50% chance of inheriting this disease and males appear to be affected much more severely than females. Although we know that *TMEM43* mutation causes ARVC, we know very little about what TMEM43 actually does in heart cells. Therefore, we have studied the basic functions of TMEM43 including cellular localization and life cycle. Understanding how the normal TMEM43 functions may provide insight into how the mutation causes heart dysfunction and may ultimately lead to a strategy to fight this disease and help patients.

Acknowledgements

I would like to express my gratitude and appreciation for Dr. Jessica Esseltine whose guidance, support and encouragement has been invaluable throughout this project. I would like to acknowledge all faculty members who taught me and helped me through my study at Memorial University. I am especially grateful to Dr. Bruno Stuyvers for his kindness and his support during my research. I would like to thank you my previous committee members, Dr. Graham Fraser and Dr. Edward Randell. I would also like to thank Dr. Dake Qi for his support throughout my first project at MUN. Finally, I am also very appreciative of my labmates who helped me in this project.

This work was supported by Memorial University School of Graduate Studies, Memorial University Faculty of Medicine and the Stem Cell Network.

I am extremely grateful to my family, who support me during my education.

Co-authorship statement

Dr. Bruno Stuyvers was very generous of his time and helped me with calcium imaging for single cells (Figure 12D). The calcium imaging presented in Figure 12A-C of this thesis was completed independently by me with a different microscope setup. Rebecca Frohlich and Grace Christopher helped me with cell culture (taking turns feeding cells on the weekend, optimizing differentiation protocols). Robert Flemmer assisted me with CRISPR-Cas9 genetic ablation and helped to optimize the immunofluorescent staining of TMEM43. I appreciate all of your help.

List of Abbreviations

ACC1- Acetyl-CoA carboxylase

AMPK - AMP-activated protein kinase

ANP - atrial natriuretic peptide

ARVC - arrhythmogenic right ventricular cardiomyopathy

AU – arbitrary units

AV node - Atrioventricular node

BSA – bovine serum albumin

CHD - coronary heart disease

CHX - cycloheximide

CRISPR - clustered regularly interspaced short palindromic repeats

cTnT/TNNT - Cardiac Troponin T

Cx43 - Connexin 43 /GJA1

Dsc - desmocollin-2

DCM - Dilated Cardiomyopathy

Dsg - desmoglein-2

DMEM - Dulbecco's minimal Eagle's medium

E8 - Essential 8™ Medium

ECL – Electrochemiluminescence

EDTA - Ethylene diamine tetra-acetic acid

FACS - fluorescence-activated cell sorting

FBS - Fetal bovine serum

GATA4 - GATA binding protein 4

GJ - Gap Junction

gRNAs – Guide RNAs

GSK3 - Glycogen synthase kinase-3

HBSS - HEPES-buffered saline solution

HCM - Hypertrophic cardiomyopathy

HCN channel: Hyperpolarization-activated Na^+ channel

HRP - Horseradish Peroxidase

$I_{Ca,L}$ /LTCC - L-type calcium channel

ID – Intercalated Disc

IF - Immunofluorescence

iPSC-CMs - Induced Pluripotent Stem Cell-Derived Cardiomyocytes

iPSCs - Induced Pluripotent Stem Cells

Isl1- ISL LIM homeobox 1

I/R injury - ischemia reperfusion injury

Klf4 - Kruppel like factor 4

LBBB - left bundle-branch block

MI – Myocardial Infarction

MHC-α - Myosin heavy chain, α isoform

MLC1/3 - Myosin light chain 1/3

MCPs: Multipotent cardiovascular progenitors

c-Myc - MYC proto-oncogene

NCX - sodium–calcium exchanger

Nkx2.5 - NK2 homeobox 5

Oct3/4 - POU class 5 homeobox 1

PBS - Phosphate-buffered saline

PAR2 - protease-activated receptor 2

qPCR - quantitative Polymerase Chain Reaction / Real-time PCR

PVC - Premature ventricular contraction

RYR2 - Ryanodine receptor 2

SA node – sinoatrial node

SAECG - Signal-averaged electrocardiography

SCD - Sudden cardiac death

SDS-PAGE – sodium dodecyl sulfate polyacrylamide gel electrophoresis

SERCA - sarco/endoplasmic reticulum Ca^{2+}-ATPase

Sox2 - SRY-box transcription factor 2

SR - Sarcoplasmic reticulum

TAC - Transverse Aortic Constriction

TBST - tris-buffered saline (TBS) and Polysorbate 20 (also known as Tween 20)

TBXT - T-box transcription factor T

TMEM43 - Transmembrane protein 43 (also called LUMA)

WB - Western blot

Table of Contents

List of Tables

List of Figures

List of Appendices

1. Introduction

1.1. The heart

The heart is a four-chambered organ, responsible for both pulmonary circulation and systemic circulation. The heart supplies oxygen and nutrients for all of the body organs including itself through the coronary arteries. The tissue of heart has three defined layers including endocardium, myocardium, and epicardium. Pumping blood is conducted via the rhythmic and coordinated contraction of the muscular myocardium, the middle cell layer of heart, located between the endocardium and epicardium (1). Approximately 75% of the normal heart tissue volume is comprised of cardiomyocytes. In addition to cardiomyocytes, the heart includes other cells such as cardiac fibroblasts, endothelial cells, smooth muscle cells, immune cells and other connective tissue cells like adipocytes (2).

The pumping of blood throughout the body generates a pressure gradient (blood pressure), which is necessary to supply blood to all tissues. There are two types of cardiac muscle cells including autorhythmic cells and contractile cells (1, 3). Regular beating of the heart depends on the cardiac conduction system that produces action potential without any stimulation, along with excitation-contraction coupling of the contractile cells in the myocardium (1).

1.2. Heart development

The heart is one of the first organs generated in the developing fetus and many heart abnormalities are embryonically lethal (4). Cardiac progenitors are specified during the early stages of gastrulation and are derived from the mesoderm embryonic germ layer. Various types of heart cells including cardiomyocytes, endothelial cells, smooth muscle

cells, as well as conduction cells arise from the differentiation of multipotent cardiovascular progenitors (MCPs) generated soon after gastrulation. One of the earliest signs of cardiovascular development is the expression of the cardiomyogenic mesoderm biomarker, mesoderm posterior bHLH transcription factor 1 (Mesp1) (4, 7).

The effective differentiation of cardiac progenitor cells to cardiomyocytes requires tight temporal and spatial organisation of several transcription factors. Multipotent progenitor cells need to replicate to increase their number and then begin differentiation to eventually generate adequate number of cardiomyocytes (4, 7). During embryonic development, cardiomyocyte progenitor cells form a linear heart tube which undergoes rightward looping to form a primitive heart structure. NK2 homeobox 5 (Nkx2.5)+, and ISL LIM homeobox 1 (Isl1)+ early cardiac progenitors are produced through the activation of canonical Wnt signaling (8). The canonical Wnt pathway (Wnt-3a and Wnt8) activates β-catenin and is inhibited through the glycogen synthase kinase 3 (GSK3). Both cell proliferation (activation of canonical Wnt signaling) and cell differentiation (suppression of canonical Wnt signaling) are necessary for embryonic heart development. Two cell layers consisting of the endocardium and the myocardium form the early embryonic heart tube. The most outer layer of heart, the epicardium, and the other cells such as cardiac fibroblasts are gradually added to the developing heart (4).

The *NKX2.5* gene encodes a homeobox-containing transcription factor which is required to complete cardiomyogenesis and mutation in this gene can cause atrial septal malformation with atrioventricular conduction defect (9). The T-box transcription factor T (*TBXT*), encoding the brachyury protein, is an embryonic nuclear transcription factor

involved in mesoderm formation and differentiation (8, 10). GATA binding protein 4 (GATA4) induces the expression of several cardiac genes including myosin heavy chain, α isoform (*MHC-α*), myosin light chain 1/3 (*MLC1/3*), cardiac troponin C, cardiac troponin I, atrial natriuretic peptide *(ANP),* cardiac sodium–calcium exchanger (*NCX1*) and cardiac m2 muscarinic acetylcholine receptor (8, 10). GATA4 overexpression has been shown to contribute to cardiac hypertrophy (8, 10). Finally, myosin heavy chain 14 (MHC14/MYH14) is a member of the myosin superfamily and is a marker of the heart and cardiomyocytes (11).

Adult cardiomyocytes are terminally differentiated. Unlike neonatal cardiomyocytes, adult cells no longer replicate. In response to stress, adult cardiomyocytes can increase only the size of the cell, without any cell number increases (8, 13). Therefore, this limited proliferative capacity is insufficient to repair heart damage in response to injury (8). Cardiomyocytes are structurally unique. The presence of two separate nuclei is a typical characteristic of this cell (12). Sarcoplasmic reticulum (SR), sarcolemma and transverse (t-) tubules as well as sarcomere are essential for the function of this cell. T-tubules are narrow invaginations of the cell membrane located at the z-line of the sarcomeres. These unique structures work together to facilitate cardiomyocyte function as outlined below (3).

1.3. Action potential

Electrical activity in the heart originates in the autorhythmic cells of the conduction system. The conduction system includes the sinoatrial (SA) node, atrioventricular (AV) node, bundle of His, bundle branches, and purkinje fibres (3). Cardiac muscle cells are electrically connected to each other via Gap Junction (GJ) channels within the intercalated

disc (14, 15). Gap junctions enable the exchange of ions and small molecules directly between adjacent cells, facilitating the transfer of electrical impulses across the myocardium (14, 15).

The cardiac action potential is a short and quick alteration in membrane potential in which the inside of the cell membrane becomes less negative (1). The electrical stimulation or excitation of the cell is carried out by the movement of several ions through specialized channels in the sarcolemma of cardiac fibers. Unlike skeletal muscle, the cardiac action potential is not initiated by nervous activity (1). Moreover, action potentials are different in autorhythmic pacemaker cells versus contractile cardiomyocytes. Autorhythmic, or pacemaker cells, can generate action potential independently, while contractile cardiomyocytes require external stimulation to initiate action potential.

Autorhythmicity within the conduction system depends on hyperpolarization-activated Na^+ (HCN) channels, which facilitate slow depolarization through Na^+ entry into the cell. When the slow membrane depolarization reaches the threshold potential, action potential is initiated via rapid Ca^{2+} influx through voltage-gated Ca^{2+} channels. The membrane potential raises rapidly to a peak, and subsequently returns to baseline in repolarization via K^+ efflux (1, 3). Membrane repolarization reactivates pacemaker HCN channels, priming the cell for another action potential (1). Therefore, pacemaker cells do not truly have a resting membrane potential.

Action potential generated within the pacemaker cells triggers the flow of Na^+ and Ca^{2+} across gap junctions to the contractile cells of the myocardium. GJ-mediated ion flow raises the membrane potential within the cardiomyocyte such that voltage-gated Na^+

channels become activated, enabling the fast influx of Na^+ ions and subsequent rapid depolarization. After reaching a maximum, the membrane potential partially repolarizes to a plateau through the simultaneous activity of voltage-gated K^+ and Ca^{2+} channels. Subsequent Ca^{2+} channel inactivation fully repolarizes the cell, returning to resting membrane potential.

1.4. Excitation–contraction (E–C) coupling in cardiac muscle:

Normal beating of the heart is achieved by organized cardiomyocyte excitation-contraction (E-C) coupling (Figure 1) (1, 3). E–C coupling is a mechanism that connects the electrical excitation of the cell membrane to a rearrangement of the cytoskeleton, ultimately resulting in cardiomyocyte contraction (3). The regulation of calcium transition into and out of the cardiac muscle cell and sarcoplasmic reticulum (SR) plays an important role in this phenomenon (1, 3). Cytoplasmic calcium concentration is precisely regulated during cardiac systole (contraction) and diastole (relaxation) to ensure rhythmic and regular cardiac output. The magnitude and duration cytoplasmic calcium are two important factors in heart contraction (3).

As outlined above, electrical activity in the heart is initiated by the autorhythmic cells of the conduction system, and is propagated through gap junction channels to the contractile cells of the myocardium (1). During cardiac systole (contraction), activation of voltage-gated L-type Ca^{2+} channels (I_{Ca},L) in the action potential plateau phase results in Ca^{2+} entry into the cell. This intracellular Ca^{2+} activates type 2 Ryanodine receptors (RYR), the most abundant calcium (Ca^{2+}) channels in the sarcoplasmic reticulum, resulting in further Ca^{2+} release from intracellular stores (calcium-induced calcium release).

Figure 1. Calcium cycling in cardiomyocytes is essential in cardiac muscle cell during contraction and excitation. Depolarization of the sarcolemma triggers the entry of calcium into the cell through the L-type calcium channels. This increase in intracellular Ca^{2+} triggers the RYR at the sarcoplasmic reticulum to release more calcium from intracellular stores (calcium-induced calcium release). The dramatic increase in cytoplasmic calcium release relieves the blocking effect of tropomyosin on actin cross-bridge binding, leading to the cardiomyocyte contraction. Figure was created by using BioRender Premium software licensed to JE, biorender.com.

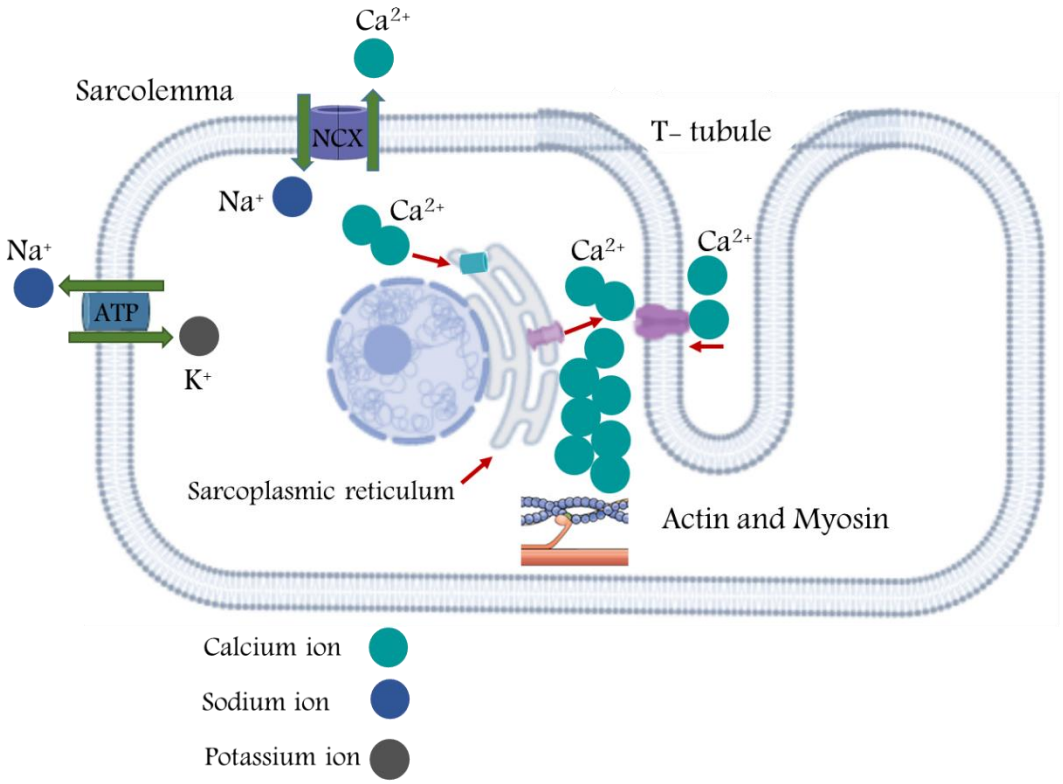
Ca2+
Sarcolemma
NCX
T– tubule
Na+
Ca2+
Ca2+
Ca2+
Na+
ATP
K+
Sarcoplasmic reticulum
Actin and Myosin
Calcium ion
Sodium ion
Potassium ion

The dramatic increase in cytoplasmic calcium triggered through calcium-induced calcium release relieves the blocking effect of tropomyosin on actin cross-bridge binding. The troponin complex is a component of the actin thin filament network and is comprised of three subunits including troponin C, troponin T, and troponin I (13). When tropomyosin is away from the blocking position, actin and myosin are able to interact at the cross bridges. When actin thin filaments are pulled inward toward the cross bridge, the sarcomere shortens and the cell contracts. The coordinated contraction of ventricular cardiomyocytes exerts pressure on the ventricles and ejects the blood through the vessels out to the rest of the body. Therefore, blood pressure depends on the amount of calcium bound to troponin. After contraction, the cell must reduce the cytoplasmic calcium level to prepare for relaxation. During diastole, sarco/endoplasmic reticulum Ca2+-ATPase (SERCA) and sodium-calcium exchanger (NCX) channels function to pump calcium back into intracellular stores or out of the cell. The reduction in intracellular calcium thus re-introduces the troponin block on actin-myosin cross bridges and facilitates cardiomyocyte relaxation. Therefore the Ca^{2+} flux balance is important for the function of cardiomyocyte E-C coupling and calcium imbalance may result in arrhythmia (3).

1.5. The intercalated disc and cardiomyocyte adhesion

The intercalated disc plays an essential role in cardiomyocyte contraction. Intercalated discs are unique structures found between the cardiomyocytes which include desmosomes, adherence junctions and gap junctions (Figure 2) (16, 17, 18). Gap junctions form large pores between adjacent cells that allow direct transmission of the electrical impulse from cell to cell across the myocardium. The gap junction protein connexin43

(Cx43) is the most widely expressed gap junction protein in the heart. Indeed, compromised Cx43 activity is widely associated with cardiac arrhythmias and Cx43 knockout animals die at birth due to heart defects (17).

Neighboring cardiomyocytes are tightly anchored together through cell–cell junctions (desmosomes and adherence junctions) that help the heart to work under constant mechanical pressure (17, 19). Desmosomes consist of three types of proteins including the desmosomal cadherins (desmogleins and desmocollins), armadillo proteins (plakoglobin and plakophilin), and plakins (desmoplakins). The cytoplasmic domains of desmoglein (Dsg)-2 and desmocollin (Dsc)-2 interact with the armadillo proteins, while desmoplakin, binds strongly to intracellular intermediate filaments, and links to Dsg-2 and Dsc-2 (18). N-cadherin forms adherens junctions and links β-catenin and plakoglobin (γ -catenin) (17, 20, 21). Desmosomes are involved in intracellular signalling pathways as well as mechanical cell attachment. For example, a mutation in several different desmosomal proteins can compromise tight cell-cell adhesion during cardiomyocyte contraction leading to cell detachment and death (22, 23). Furthermore, plakoglobin mutation causes this protein to redistribute from the cell membrane into the nucleus. This altered localization disrupts canonical Wnt–β-catenin signaling pathway and triggers pathological gene transcription ultimately leading to adipofibrogenesis (22).

Figure 2. The intercalated disc provides structural support and electrical coupling to cardiomyocytes. Desmosome, adherens junction and gap junction form the intercalated disc between two cardiomyocytes. Desmosomes form strong connections for mechanical attachment between cells of the myocardium while gap junctions enable the rapid conduction of electrical signals between adjacent myocytes. Figure was created by using BioRender Premium software licensed to JE, biorender.com.

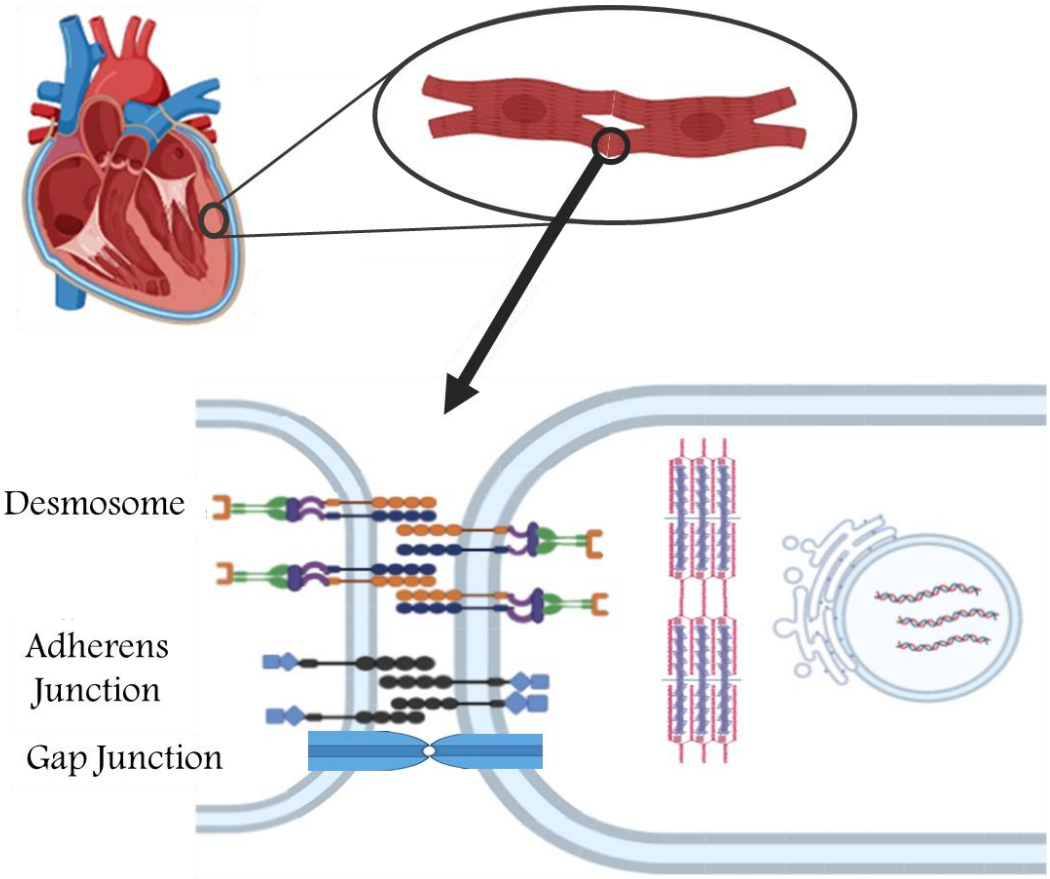
Desmosome
Adherens Junction
Gap Junction

1.6. Heart disease

According to the most recent data from 2012/13, heart disease is the second leading cause of death of Canadians (24). Men are generally affected earlier than women (men aged 55-64 vs 65-74 years for women). About 669,600 (3.6%) Canadian adults aged 40 years and older live with diagnosed heart failure. Encouragingly, the incidence of death due to heart disease appears to be dropping in western countries (24).

Cardiovascular impairment can be caused by failure of one or more of the main mechanisms including pump failure, flow obstruction, regurgitant flow, shunted flow, disorders of cardiac conduction, and rupture of the heart or a major vessel (25). Genetics and environmental factors both play important roles in the development and pathogenesis of heart disease (25). Heart disease can be categorized as heart failure, cardiomyopathy, arrhythmias, ischemic heart disease, hypertensive heart disease, congenital heart disease, valvular heart disease and pericardial disease (25). Below I will go into more details regarding the various cardiomyopathies, arrhythmias and ischemic heart disease.

1.6.1. Ischemic heart disease

Ischemic heart disease and related coronary artery disease occurs primarily in response to the formation of obstructive atherosclerotic plaque within the coronary arteries. These atherosclerotic plaques restrict blood flow to the heart muscle (ischemia), which results in reduced oxygen and nutrients for the cardiomyocytes of the ischemic area. If unstable, the atherosclerotic plaque may rupture, resulting in hemorrhage and myocardial infarction (heart attack) (25). Ultimately the restricted availability of nutrients, as well as myocardial infarction, results in cardiomyocyte death.

1.6.2. Heart failure and congestive heart failure

Heart failure is the inability of the heart to pump oxygen-rich blood to the body as effectively as it should. Consequently, the body cannot function optimally as it lacks adequate oxygen, energy and nutrients. Several conditions such as coronary artery disease, myocardial infarction, and cardiomyopathy can damage or weaken the heart and lead to heart failure (25, 26).

1.6.3. Cardiomyopathy

Cardiomyopathy is a condition in which the heart muscle is damaged and usually leads to heart failure due to an inadequate number of functional cardiomyocytes. Mechanical or/and electrical impairment of the heart can result in cardiomyopathy along with heart enlargement (25). Heart failure occurs due to the inability of the heart muscle to generate adequate cardiac output (CO) and ejection fraction, which means the heart can no longer effectively pump blood throughout the body 27). There are both acquired and inherited forms of cardiomyopathy, however, many cardiomyopathies have a strong genetic component. As detailed later, inherited mutations can compromise cardiomyocyte contraction, cell-cell adhesion, cytoskeleton integrity, or dysregulated intercellular ion transport. Shortness of breath, fatigue, and arrhythmias are important signs and symptoms of cardiomyopathy (28). There are three pathological cardiomyopathy classes: dilated cardiomyopathy, hypertrophic cardiomyopathy and restrictive cardiomyopathy (25).

Dilated Cardiomyopathy (DCM) is characterized by heart enlargement and dilation of ventricles along with abnormality in cardiac contraction resulting in reduced ejection fraction. Therefore, systolic dysfunction is a feature of DCM. Arrhythmogenic right

ventricular cardiomyopathy (ARVC) is classified in this group of cardiomyopathies. It is an inherited, right ventricular failure and impaired rhythm (ventricular tachycardia) (25, 28, 29). ARVC is described in much more detail below.

Hypertrophic cardiomyopathy (HCM) is associated with heart enlargement and a thick heart wall. Unlike DCM, HCM does not have a dilation and the left ventricle is unable to appropriately fill due to the heart wall thickness. This condition leads to diastolic dysfunction (25, 28). DCM has a large genetic component; however high blood pressure and aging can also lead to hypertrophic cardiomyopathy.

Restrictive cardiomyopathy is rare. This type of cardiomyopathy is characterized by extreme heart stiffness. The stiffness makes the heart unable to expand and fill accurately. It occurs mostly in people of advanced age (25).

1.6.4. Arrhythmias

Arrhythmia is defined as the abnormal rate and rhythm of the heartbeat. Abnormalities in the heart conduction system leads to aberrant cardiac excitation and contraction or so-called arrhythmias. Arrhythmias can be inherited or arise due to heart damage from various diseases like myocardial infarction. Also, coronary heart disease, ventricular injury, or electrolyte imbalance in the body can cause arrhythmia. Both inherited and acquired arrhythmias manifest in fast heart rate (tachycardia, > 100 beats per minute), slow heart rate (bradycardia, < 60 beats per minute) or irregular heart beating (fibrillation) (27). Arrhythmia can be detected by electrocardiography (25). Patients suffering from an arrhythmia may have severe or mild symptoms ranging from sudden cardiac death to weak palpations or even nothing at all.

1.7. Arrhythmogenic Right Ventricular Cardiomyopathy (ARVC)

1.7.1. ARVC pathophysiology

ARVC is a form of dilated cardiomyopathy with thinning of the inferior, apical, and infundibular walls of the heart (30). ARVC is characterized by fibrofatty replacement of the myocardium and ventricular arrhythmias. This disease generally affects adults and is more severe in men versus women and with variable penetrance (30, 31). This means that some ARVC patients will live a relatively normal lifespan with mild disease phenotypes while others may die at a very young age. Patients are often asymptomatic in the early phase of the disease, however ARVC can lead to SCD or cardiomyopathy resulting in heart failure (16, 32, 33).

In 1982, Marcus and colleagues reported the first case of ARVC (34) and there are now many reported cases across the world especially in endemic regions such as Italy and Newfoundland in Canada. Approximately half of all ARVC cases have a genetic component, in more than a dozen different genes including desmosomal or non-desmosomal genes (22, 32). Many of these genetic mutations are autosomal dominant, meaning that patients have approximately 50% chance of passing on the affected allele to their children (30, 35).

Physical exercise, which increases heart activity and blood pressure, exacerbates ARVC symptoms (36). Dopamine, norepinephrine and epinephrine create a group of hormones called catecholamines that have several target organs within the body including the heart (37, 38). They can cause elevated heart rate and blood pressure as well as increased

breathing rate. In individuals with ARVC, catecholamines can also trigger or exacerbate cardiac rhythm disorders or arrhythmia (39, 40).

1.7.2. ARVC diagnosis

Abnormal electrocardiography is a hallmark of ARVC. Ventricular arrhythmias can range from frequent premature ventricular beats to ventricular tachycardia with left bundle-branch block (LBBB) pattern and ventricular fibrillation leading to cardiac arrest (30). Right ventricular enlargement is common, and enlarged left ventricle can also be observed. The dilated RV causes dysfunction and abnormalities of regional wall-motion such as systolic akinesia or dyskinesia or diastolic bulging (41). Eventually, patients succumb to sudden arrhythmogenic cardiac death or progressive heart failure.

There is not any single test to identify individuals with ARVC. Clinicians utilize several medical exams and task force criteria to diagnose ARVC (34). Electrocardiogram (ECG) and echocardiography are the first test usually requested for suspected patients. However, other tests, including signal-averaged ECG (SAECG) and 24-hour Holter monitors are also performed to evaluate patients. Some of the task force criteria related to ECG and 24-hour monitoring are as follows: QRS >110 in V1, V2 and V3; premature ventricular contractions (PVCs); and left bundle branch block; abnormalities of repolarization and depolarization; inverted T waves in right precordial leads (V1, V2, and V3); epsilon wave; and ventricular tachycardia. Heart enlargement and the size and shape of the ventricular free walls and septum are also important parameters for detecting ARVC (34). Other task force characterizations include histological characterization of heart wall wherein pathologists quantify the fibrofatty replacement of myocardium in free wall of RV.

Finally, as ARVC has a strong genetic component, family history (especially in a first-degree relative) is a major factor in diagnosing ARVC.

1.7.3. Cardiomyocyte cell death in ARVC

One major mechanism of ARVC involves mutations in components of the intercalated disc (ID), which link adjacent cardiomyocytes and lend strength and stability to the cardiac wall and propagates electrical activity across the heart (23). Almost 60% of ARVC patients have mutation in desmosomal genes including plakophilin-2, desmoplakin and desmoglein-2 (19). Desmosomal dysfunction weakens the normally strong adhesion between cardiomyocytes, causing detachment of cardiomyocytes from each other (40). This detachment can lead to cell death and progressive atrophy of the myocardium accompanied by fibrofatty substitution (22, 23).

Desmoglein-2 is essential for the assembly of the desmosome and mutation in this protein is linked to cardiomyocyte cell death followed by fibrofatty substitution and severe ARVC (16). There is also a relationship between the desmosomal PKP2 and expression of the NaV1.5 sodium channel, which can influence the velocity of action potential (43, 44). The expression level of the gap junction protein Cx43 has been shown to be decreased in arrhythmogenic cardiomyopathy patient hearts (43). Although the majority of inherited ARVC is linked to mutations in desmosomal proteins, ARVC can also be caused by mutations in non-desmosomal proteins such as the RYR2 calcium channel, and the nuclear envelope proteins lamin A/C and TMEM43 (43, 44).

1.7.4. Fibrofatty replacement in ARVC

A primary pathological outcome of ARVC is replacement of right ventricular myocardium with fibrous-adipose tissue (fibrofatty tissue) in the right ventricular free wall (46). The fibrofatty replacement of the myocardium is the heart's attempt to heal the damaged tissue (45). The fibrofatty replacement causes wall thinning and aneurysmal dilatation, typically localized in the inflow tract (46, 45). Additionally, the invasion of non-excitable fibrofatty tissue can interrupt electrical coupling within the conduction system, or interfere with the electrical transmission across the ventricular myocardium. This can lead to the formation of epsilon waves, right bundle branch block, delayed action potentials and ultimately arrhythmia (30).

1.8. Nuclear envelope proteins and ARVC

The cytoskeleton of a cell is comprised of cytoskeletal filaments including microtubules, actin filaments, and intermediate filaments. The shape of the cell and organization of cell's compartments depend on cytoskeleton (47). Nuclear lamins are a type of intermediate filaments that interact with inner nuclear membrane proteins to produce the lamina. The nuclear lamina includes lamin A and lamin B and has an essential role in supporting nuclear envelope structural integrity and transportation within this membrane. The lamina provides a scaffold or stable filament network for chromatin, DNA replication and gene expression (48, 49). ARVC and other forms of cardiomyopathy are associated with mutations in several nuclear envelope and associated genes. The LINC complex including nucleoskeleton and cytoskeleton physically support the nucleus and play an important role in the structure of the nucleus such as chromatin localization. Therefore, the

proteins within the inner nuclear membrane, along with those connecting the nucleoskeleton to cytoskeleton, directly play a role in gene expression and cell function (48). Lamin A/C is essential for cardiomyocyte function and Lamin A/C heterozygous mutant mice fail to mount appropriate hypertrophic response when subjected to pressure overload by transverse aortic constriction (TAC) (50). Other nuclear envelope proteins including TMEM43 and Desmin are involved in ARVC as outlined below (16).

1.8.1. TMEM43

Transmembrane protein 43 (TMEM43) or LUMA is a non-desmosomal protein located at the inner nuclear membrane of several cell types (48, 49). TMEM43 is a conserved protein and is expressed in various tissues of human body. However, the expression level of TMEM43 in different tissues is variable (49). Human TMEM43 is a 400 amino acid protein with a molecular mass of 44.8 kDa. The *TMEM43* gene contains 13 exons on chromosome 3 (3p25.1) (49). *In silico* analysis suggests that this protein has four hydrophobic membrane-spanning domains, and a large hydrophilic domain located between the first and second predicted transmembrane domains (49).

Very little is currently understood about the basic life cycle and function of TMEM43. TMEM43 links to emerin and lamin A/C in the nuclear envelope (NE) region (Figure 3). TMEM43 association with Lamin A/C is thought to be necessary for localization of TMEM43 in the NE (50). In addition to the nuclear envelope, TMEM43 has been reported to localize to the endoplasmic reticulum, intercalated disc, gap junctions and other diverse intracellular compartments (51).

Figure 3. TMEM43 intracellular localization and known protein-protein interactions. The illustration shows the TMEM43 localization and interaction with the other proteins in the nuclear envelope. Within the nuclear envelope, TMEM43 interacts with lamin and emerin. The large hydrophilic loop of TMEM43 is thought to protrude into the endoplasmic reticulum. Figure was created by using BioRender Premium software licensed to JE, biorender.com.

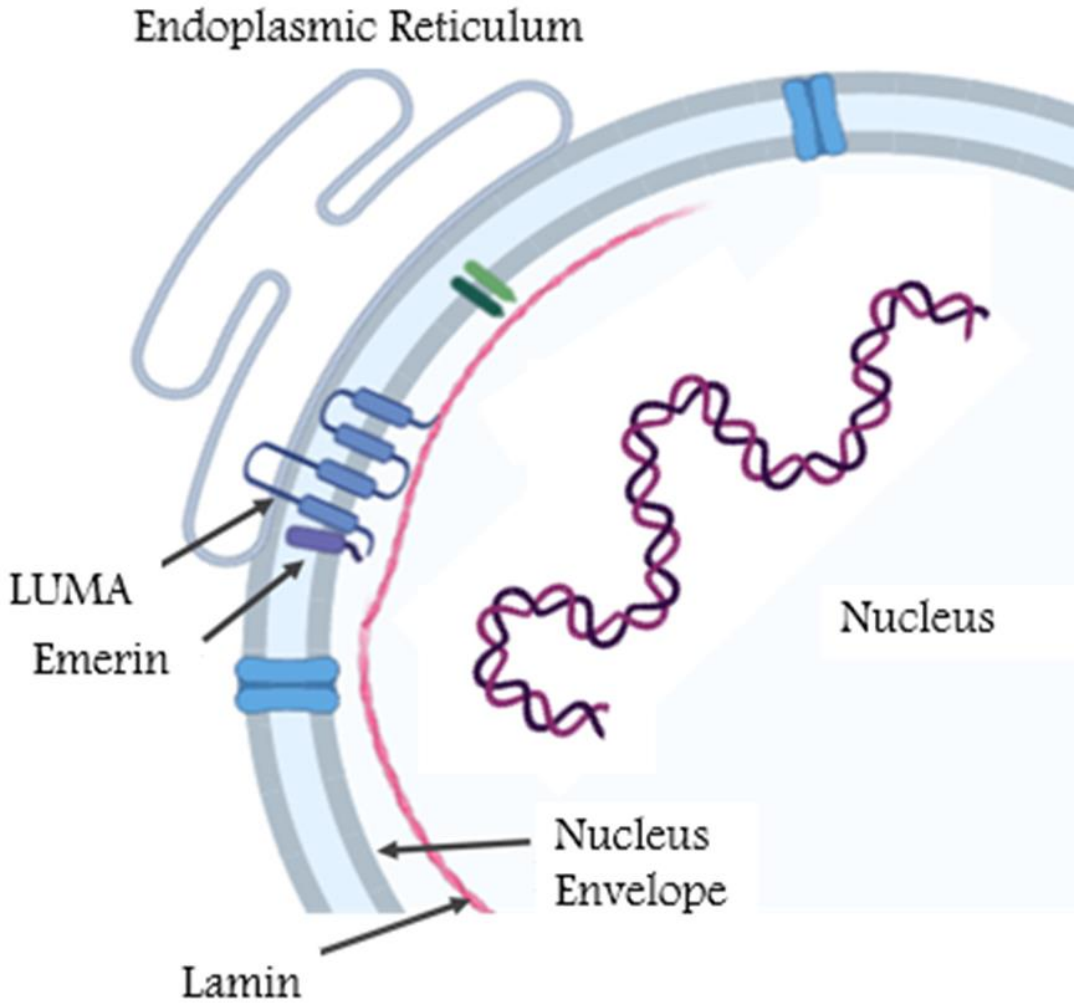
Endoplasmic Reticulum
LUMA
Emerin
Nucleus
Nucleus
Envelope
Lamin

The localization of TMEM43 is further complicated by the fact that missense mutations may alter the localization of the protein (48). For example, while wild type TMEM43 has been shown to localize to the nuclear envelope of murine cardiomyocytes, overexpressed TMEM43-S358L is located throughout the cytoplasm (51).

1.8.2. TMEM43-associated ARVC5

In 2008, researchers at Memorial University of Newfoundland found an autosomal dominant mutation in the *TMEM43* gene (c.1073C>T, p.S358L) within a cluster of patients suffering from ARVC (denoted ARVC5) (52). This *TMEM43* mutation was recognised in 15 Canadian families suffering from ARVC5 (52). The same *TMEM43* mutation was subsequently reported in some European countries including Germany (53) and Denmark (54). Also group of scientists at University of Toronto reported this mutation in non-Newfoundland populations (55).

The S358L mutation occurs in the third transmembrane domain of the TMEM43 protein (22, 48). This gene variant is fully penetrant, meaning that every single individual who inherits this diseased allele will develop ARVC (56). Since ARVC5 is an autosomal dominant disorder, only one mutant allele needs to pass from one of the parents to offspring in order to generate disease in the next generation. Thus, when one of the parents is affected, the child has a 50% chance of inheriting the mutated gene. ARVC5 is much more severe in male patients than female patients, with higher rates of sudden cardiac death, heart failure requiring transplant and lower overall lifespan (52).

1.8.3. Current models of TMEM43-associated ARVC5

While animal models have been used for decades to understand human physiology and pathophysiology, they sometimes fail to recapitulate key aspects of human disease. *TMEM43* knockout mice appear phenotypically normal with no apparent cardiac pathology, no alteration in cardiac function or remodelling under pressure overload compared to wild type littermates (50). Meanwhile, TMEM43-S358L transgenic mice exhibit some cardiac remodelling found in ARVC5 patients and reduce the life span (56). Cardiomyocyte cell death in TMEM43-S358L transgenic mice is due, in part, to aberrant activation of glycogen synthase kinase-3β. Pharmacologically blocking GSK3β normalizes the survival of transgenic mice (56). However, TMEM43-S358L transgenic mice do not suffer from sudden cardiac death, nor do they display sex differences so prevalent in the human population (56). Therefore, additional models are necessary to complement these animal studies in order to understand ARVC in human patients (57, 58).

1.9. Cell model in cardiovascular disease

1.9.1. Modelling cardiovascular disease with stem cells

Stem cells are unspecialized cells with the unique ability to differentiate into various types of cells. Induced pluripotent stem cells (iPSCs) are created by "reprogramming" terminally differentiated cells, such as skin or blood cells (59). Reprogramming is achieved by transducing cells with only four transcription factors, POU class 5 homeobox 1 (*POU5F1*, encoding for Oct3/4), SRY-box transcription factor 2 (SOX2), MYC proto-oncogene (c-MYC), and Kruppel like factor 4 (KLF4) (Yamanaka factors) (59, 60). These reprogrammed iPSCs show an embryonic-like pluripotent state with an ability to differentiate to every type of human cell in the body, including cardiomyocytes (59, 61).

Moreover, by utilizing gene editing technologies including CRISPR-Cas9 scientists are able to create targeted gene knockouts or fine gene editing on a isogenic background. Because iPSCs can be generated from healthy adults as well as those with disease, they are a powerful model to understand human disease in a personalized, translational capacity.

1.9.2. Attributes of iPSC-derived cardiomyocytes

Differentiating iPSCs to cardiomyocytes may result in myocytes with nodal, atrial, and ventricular type of action potential properties (62, 63). During the differentiation of pluripotent stem cells to cardiac fate (Figure 4), several transcription factors such as T/Brachyury for primitive streak mesoderm, Mesp1 for cardiogenic mesoderm, and Nkx2.5, Tbx5/20, Gata-4, Mef2c, and Hand1/2 for cardiac mesoderm should be expressed (7). Mesp1 directly binds to regulatory DNA sequences in the promoters of many members of the core cardiac regulatory network, including Nkx2.5, causing development of mesoderm precursors of the cardiovascular lineage (7). The α-actinin, α-myosin heavy chain, and the cardiac isoform of Troponin-T are structural protein in mature cardiomyocytes. Several receptors and pathways such as Notch and Wnt expand the pool of $Nkx2.5^{+}$, and $Isl1^{+}$ early cardiac progenitors (64). GSK-3 inhibition, p38 MAPK inhibition, and PI3K/Akt activation may enhance cardiac progenitor proliferation (65, 66).

Pluripotent stem cell-derived cardiomyocytes have several structural similarities to adult cardiomyocytes, including sarcomere and intercalated disc. A major limitation to the use of iPSC-derived cardiomyocytes (iPSC-CMs) is the maturity and purity of the resulting culture. iPSC differentiation into cardiomyocytes generates primarily immature cardiomyocytes, reminiscent of fetal cells (67). Therefore, these cells lack key attributes of

mature cardiomyocytes. For example, iPSC-CMs are morphologically different from mature cardiomyocytes as they are not rod shaped (12). The presence of several mitochondria and multinucleation are common in adult cardiomyocytes (20%), although multinucleation is not usual in pluripotent stem cell-derived cardiomyocytes (less than 1%). Furthermore, although adult ventricular cardiomyocytes are contractile cells, they are not able to contract spontaneously, while iPSC-CMs are able to spontaneously contract. High levels of hyperpolarization-activated cyclic nucleotide-gated channel 4 (HCN4) in the sarcoplasmic membrane of iPSC-CMs makes it possible to initiate contraction without external stimulation (67). Mature ventricular cardiomyocytes exhibit significantly higher membrane hyperpolarization at resting membrane potential compared to iPSC-CMs (67). iPSC-CM membrane repolarization initiates immediately after depolarization by rapid delayed-rectifier potassium currents. On the other hand, mature ventricular cardiomyocytes exhibit a plateau phase via the L-type calcium channel (LTCC) (67).

Pluripotent stem cell-derived cardiomyocytes express the early cardiac-specific transcription factors GATA-4, Nkx2.5, Isl-1, Tbx-5, Tbx-20, and Mef2c (63, 64). These cells also express cardiac and muscle-specific proteins such as cardiac troponins T, and I, sarcomere myosin heavy chain, atrial- and ventricular myosin light chains, atrial natriuretic peptide, creatine kinase-MB, and myoglobin (8). They also express different calcium channels like L-type calcium channel (68). Therefore, while human iPSC-derived cardiomyocytes do not entirely recapitulate the cellular and structural complexities of the human heart, they are still a useful tool to investigate the consequence of genetic mutation on cardiomyocyte differentiation and function.

Figure 4. Generation of iPSC from dermal fibroblast. Adult human dermal fibroblasts are reprogrammed into induced pluripotent stem cells (iPSCs) through overexpression of the 4 Yamanaka factors (Oct3/4, Sox2, c-Myc, and Klf4). iPSCs can then be differentiated into cardiomyocytes through several discreet steps. Activation of canonical Wnt signaling pathway followed by inactivation of this pathway is an important phase in this procedure. Resulting iPSC-derived cardiomyocytes recapitulate many key aspects of cardiomyocyte function, including expression of key cardiac genes, as well as contraction-coupling. Figure was created by using BioRender Premium software licensed to JE, biorender.com.

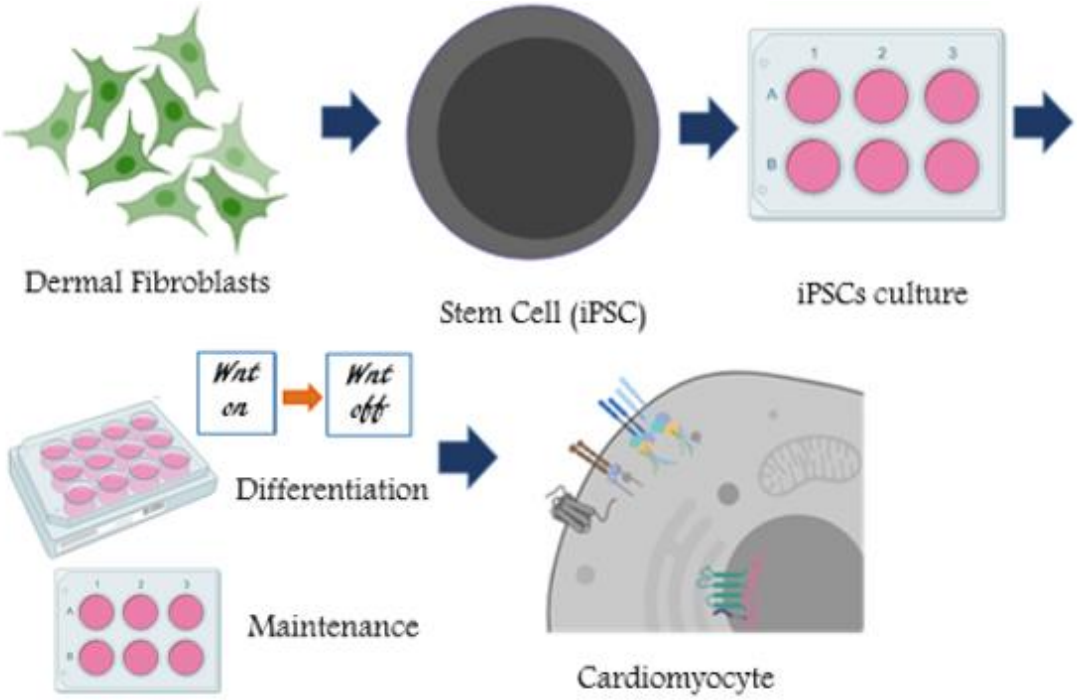
Dermal Fibroblasts
Stem Cell (iPSC)
iPSCs culture
Wnt on
Wnt off
Differentiation
Maintenance
Cardiomyocyte

1.10. Rationale and objectives

The molecular role of TMEM43 is poorly understood and how it contributes to cardiomyocyte dysfunction is virtually unknown. Because current models of TMEM43-associated ARVC fail to recapitulate key disease aspects, a human-oriented model is necessary. We will uncover fundamental aspects of TMEM43 protein life cycle and function through the following three objectives:

1) Determine the half-life and localization of TMEM43 in wild type human AD293 cells and iPSCs by cycloheximide chase analysis, western blotting and immunofluorescence staining respectively.

2) Evaluate iPSC-derived cardiomyocytes for TMEM43 and cardiac-specific gene expression, as well as contraction-coupling using qPCR, western blotting, immunofluorescence staining and calcium imaging.

3) Investigate the effect of TMEM43 genetic ablation in human AD293 cells, iPSCs and iPSC-derived cardiomyocytes by CRISPR-Cas9.

2. Materials and Methods

2.1. Human AD293 cell culture

All studies were approved by the Human Research Ethics Board (HREB) #2018.210 and the Memorial University of Newfoundland Biosafety certificate #M-007. Human AD293 cells (240085, Agilent, Santa Clara, USA) are derived from standard HEK293 cells. Cells were housed at 37°C in a humidified cell culture incubator supplemented with 5 % CO2 and fed with Dulbecco's Modified Eagle Medium (DMEM, 319-015-CL, Wisent, Saint-Jean-Baptiste, Quebec, CA) supplemented with 10% (V/V) fetal bovine serum (FBS, 12483020, Thermofisher Scientific, Waltham, Massachusetts, US) and 1% penicillin/streptomycin (P/S, 15070063 , Thermofisher Scientific). The cells were passaged when the cell confluency reached 80% or almost covered the bottom surface of the dish. Before passaging, the medium was removed by aspirator and the cells were washed by phosphate buffered saline (PBS, without calcium and magnesium) (A1285601, ThermoFisher Scientific). Cells were then incubated in trypsin-EDTA solution (25200056, ThermoFisher Scientific) for 5 minutes at 37°C in order to dissociate the cells from the container. After trypsinization, 5 ml of the fresh complete medium was added to the flask to inactivate trypsin. The flask was gently tapped until the cells released from the flask. After that, the cell-clumps were broken by gently pipetting up and down. Cells were passaged at a ratio of 1:20 into a new cell culture dish with fresh media.

2.2. Human Induced Pluripotent stem cells

Two different cell lines were employed in this study in order to find a possible relation between sex (XX/XY) and cellular pathogenicity in ARVC. The 43Q-iPSC was

reprogrammed from dermal fibroblast cells from a 32-year-old apparently healthy Caucasian female (69) while the GM25256-iPSC was derived from dermal fibroblast from an apparently healthy 30-year-old Japanese male (GM25256, NIGMS Human Genetic Cell Repository).

2.2.1. iPSC culture and passaging

All human iPSC cell lines were cultured in Essential 8 (E8) medium (A1517001, ThermoFisher Scientific) on Geltrex-coated cell culture dishes (A1413302, ThermoFisher). Cells were housed in a humidified 37ºC cell culture incubator supplemented with 5% CO_2 and were fed daily to replace the nutrients and growth factors necessary to maintain pluripotency (70). Cells were visually inspected daily to ensure iPSCs were healthy, with little or no spontaneous differentiation. Typical healthy iPSCs grow in tightly packed colonies with highly refractive borders, low cytoplasm to nuclear ratio and prominent nucleoli (70).

Cells were passaged when they reached greater than 60% confluency, approximately every 5 days. Cell culture dishes were pre-coated for one hour at 37 ºC with Geltrex diluted 1:100 in DMEM (319-015-CL, Wisent). For clump passaging to maintain cultures, cells were incubated in Gentle Cell Dissociation Buffer (13151014, ThermoFisher Scientific) until colonies could be seen under the microscope to be breaking apart into smaller clumps of 5-10 cells, approximately 5min. Clumps were then gently removed from the dish with a sterile cell scraper and re-plated into fresh Geltrex-coated dishes at a split ratio of 1:20 in Essential 8 media (70). In preparation for cardiomyocyte differentiation, iPSCs were passaged as single cells using Accutase (07922, STEMCELL Technologies BC, Canada)

until colonies floated off of the dish, approximately 8min. Cells were centrifuged at 300x g for 5min and resuspended in Essential E8 medium supplemented with 10 µM Rho Kinase inhibitor or Y-27632 ROCK Inhibitor/Y-27632 (72308, STEMCELL Technologies) to support single cell iPSC survival (75). Cells were re-seeded into a fresh Geltrex coated 12-well dish at a density of 0.8 x 10^6 cells per well.

2.3. TMEM43 CRISPR-Cas9 gene ablation

TMEM43 knockout AD293 cells and human iPSCs were created as described previously (71, 72). Two sgRNAs targeting human *TMEM43* were designed using the Sanger Institute CRISPR finder (http://www.sanger.ac.uk/htgt/wge/) (Sanger sgRNA ID 950611662 (5′-TGGCGCCTTACGGACATCCA-3′); Sanger sgRNA ID 950611647 (5′-ACGGCAACCTCATTGGCTGA-3′). These two sgRNAs were selected based on their low exonic off-target predictions. The two sgRNAs were cloned into either the pSpCas9(BB)-2A-GFP (PX458) or pSpCas9(BB)-2A-Puro (PX459) V2.0 plasmids (Addgene, Cambridge, MA, USA). These plasmids encode for the Cas9 protein along with a cloning backbone for a single guide RNA (sgRNA) and selection marker (PX458:GFP or PX459:puromycin selection) (73). Human AD293 cells and iPSCs were both transfected using the Mirus TransIT®-LT1 Transfection Reagent (Mirus Bio LLC, Madison, WI, USA; MIR-2304) according to the manufacturer's instructions. After transfection, cells were selected for puromycin resistance with 2 µg/mL puromycin treatment (A1113803, ThermoFisher Scientific). Single GFP-expressing cells were sorted using fluorescence activated cell sorting (FACS). The resulting clonal populations were examined for

TMEM43 protein ablation via immunocytochemistry, Western blotting and quantitative RT-PCR.

2.4. Differentiation of human iPSCs into contracting cardiomyocytes

Human iPSCs were differentiated into cardiomyocytes as has been previously described (56). iPSCs were seeded as single cells in Essential 8 supplemented with Y-27632 ROCK inhibitor at a density of 2 x 10^5 cells/cm^2. After 24 hours, the medium was changed with Essential 8 without Y-27632 ROCK inhibitor. The cells were kept in this medium for 24 hours. After that, the medium was changed to RPMI 1640 medium (11875093, ThermoFisher Scientific) supplemented with B27 (minus insulin) (A1895601, ThermoFisher Scientific) and 5 μM CHIR (72054, STEMCELL Technologies). Forty-eight hours later, media was changed to RPMI 1640 with B27 supplemented with 4 μM IWP2 (72124, STEMCELL Technologies). After another forty-eight hours, cells were incubated in RPMI 1640 with B27 with no additional supplements. This final media was replaced every two days until cells begin to contract, usually after about 14 days.

2.5. Western Blotting

2.5.1. Extraction of proteins from cell culture

Cell culture media was discarded, and the cells were washed twice with ice-cold phosphate buffered saline solution (PBS, 140 mM NaCl (600-082-DG, Wisent), 2.6 mM KCl (P330-500, Fisher Scientific), 1.4 mM KH2PO4 (BP362500, Fisher Scientific)). PBS was discarded and ice-cold lysis buffer was added (150 mM NaCl; 1.0% Triton X-100; 50 mM Tris pH 8.0). After 10 minutes incubation at 4°C, the cells were collected with cold plastic cell scraper and transferred to the microcentrifuge tube. Lysates were centrifuged at

14000 x g for 10 minutes at 4°C to pellet the insoluble material. The supernatant as cell lysate was kept at -20°C until further use.

2.5.2. Protein assay

Protein concentration was determined in duplicate using the Pierce BCA Protein Assay Kit (PI23225, ThermoFisher Scientific) according to the manufacturer's instructions. Colorimetric detection was performed on a VICTOR plate reader (model 2030, Perkin Elmer, Waltham, Massachusetts, US) at 595nm light. Protein concentrations were extrapolated using a bovine serum albumin (BSA; B4287, Sigma, MO, USA) standard curve of known protein concentrations (Standard curve from 0-2 µg/ml). Protein concentration was interpolated from the BSA standard curve using the formula $y = mx + b$, where m is the slope, b is the y-intercept and x is the unknown protein concentration.

2.5.3. SDS-PAGE

Proteins were separated via sodium dodecyl sulfate polyacrylamide gel electrophoresis (SDS-PAGE). For each sample, equal amounts of protein were loaded into each well and the volume of every single sample was normalized using PBS. Protein denaturation and loading buffer (10% SDS, 50% Glycerol, 0.5% Bromophenol Blue, 250 mM Tris-HCl, pH 6.8, 5% 2-mercaptoethanol) was added to each sample prior to separation via SDS-PAGE. After that samples were mixed well and placed at 100°C for 10 minutes. Protein samples were loaded into a 7.5% poly-acrylamide gel (EC-890, National Diagnostics, Atlanta, Georgia, US) and run at 100 volt using the Mini Trans-Blot® Cell (1658005, Bio-rad, CA, USA). The gel was transferred to the nitrocellulose membrane (0.45 µm pore size, 1620115, Bio Rad) at 100 volt for an hour at 4°C.

2.5.4. Immunoblotting

The membrane was blocked with 3% non-fat milk (Carnation®) diluted in Tris Buffered Saline with Tween 20 (TBS-T) (15.2 mM Tris HCL, 46.2 mM Tris base (1610719, Bio Rad), 150.6 mM NaCl (600-082-DG, Wisent), and 0.1% Tween 20 (BP337100, Fisher BioReagents)) for 1 hour at room temperature. After blocking, the membrane was incubated with primary antibody diluted in the same blocking buffer described above overnight at 4°C. The following primary antibodies were used: Rabbit anti TMEM43 ([1:5000], ab230213, Abcam, Cambridge, UK); Rabbit anti-connexin43/Cx43 ([1:5000], C6219, C6219, Sigma-Aldrich, St. Louis, Missouri, US); mouse anti cardiac troponin T/cTnT ([1:5000], ab8295, Abcam); Mouse anti Glyceraldehyde 3-phosphate dehydrogenase/GAPDH ([1:5000], CAB374, CAB374, ThermoFisher Scientific). Excess primary antibody was washed from the membrane with TBS-T (3 washes of 10 minutes each) and membranes were incubated with horseradish peroxidase (HRP)-labeled secondary antibody diluted in 5% BSA solution in TBS-T for one hour at room temperature. The following secondary antibodies were used: Goat anti mouse-HRP ([1:5000], 31430, ThermoFisher Scientific) and goat anti rabbit-HRP ([1:5000], 31460, ThermoFisher Scientific). Excess secondary antibody was washed from the membrane with TBS-T (3 washes of 10 minutes each) and exposed using ECL (1705061, Bio Rad). Blots were visualized using the ImageQuant LAS 4000 series (28 9558 10, GE Healthcare, Chicago, Illinois, US).

2.5.5. Immunoblot analysis

Western blots were analyzed by densitometry using FIJI software (NIH.gov) (74). Protein loading was accounted for across all samples using the house keeping protein GAPDH. The integrated density of each sample was calculated by FIJI and normalized to the integrated density of GAPDH of the corresponding sample.

2.5.6. TMEM43 Half-life in AD293 cells (cycloheximide chase)

In order to determine TMEM43 protein half-life, wild type AD293 cells were seeded at 2.5 x 10^4 cells/cm^2 and treated with 25 µM cycloheximide (CHX, C1988, Sigma-Aldrich, St. Louis, Missouri, United States) for 0, 1, 2, 4 and 8hours to inhibit protein synthesis. After CHX treatment, cell lysates were collected and subjected to SDS-PAGE and Western blotting as outlined in section 2.5.

2.6. Quantitative Real-time PCR (qRT-PCR)

2.6.1. RNA Extraction and cDNA Synthesis

Total RNA was isolated using Invitrogen PureLink RNA Mini Kit (12183020, Thermo Fisher Scientific) according to the manufacturer's instructions. Genomic DNA was degraded through on-column DNaseI digestion ((EN0521, Thermo Fisher Scientific). Extracted RNA was kept in -80°C. The quantity and quality of extracted RNA of each sample was measured by nanodrop (NanoDrop™ 2000/2000c Spectrophotometers, ThermoFisher Scientific). High quality RNA is assessed as having a λ260/280 ratio of ~2.0 and a λ260/230 ratio of ~2.2. 500 ng of extracted RNA was used to generate cDNA by using the High-Capacity cDNA Reverse Transcription Kit (4387406, Thermo Scientific). cDNA was stored at -30°C until use.

2.6.2. Quantitative Reverse Transcription Polymerase Chain Reaction (qPCR)

Gene expression was assessed via quantitative qPCR using SYBR green (1725124, Bio-rad). Primer sequences are outlined in Table 1. The reference gene was *GAPDH* while target genes included *TNNT*, *MYH14*, *NKX2.5*, *TBXT*, *GATA4*, *MESP1*, *TMEM43* and *GJA1* (Cx43). qPCR was performed in a ViiA 7 Real-Time PCR thermocycler (Applied Biosystems, USA). Cycle conditions were as follows: pre denaturation 95°C, 5 minutes, initial denaturation 95°C, 15 seconds, primer annealing/extension 62°C, 60 seconds, 40 cycle. The melting curves of amplicons were gained with temperatures ranging from 62°C to 95°C with a 0.05°C increase in temperature every second.

Values were normalized to undifferentiated iPSCs or normal human adult male right ventricular heart RNA (R1234139-50, Cedarlane, Burlington, ON, Canada). Three technical replicates were included across each of three biological replicates.

Table 1. Primer sequences for qPCR

	Name	Sequence (5′ to 3′)	Annealing Temp (°C)
1	*GAPDH*	F: TGCTTTTAACTCTGGTAAAG R: CACTTGATTTTGGAGGGATC	62
2	*TNNT*	F: AGATGGCCCAATGGAGGAGTC R: TCCGGTGGATGTCATCAAAGTC	62
3	*MYH14*	F: TTCGGAGCTTCACGGGTTCGAG R: CATGTCCTCGGCCTTGCTGAAC	62
4	*TMEM43*	F: CAAGCTGGAGGACCCTCATGTG R: ACAGGAAACCAGTCCACCAAGG	62
5	*GJA1* (CX43)	F: GGTCTGAGTGCCTGAACTTGCCT R: AGCCACACCTTCCCTCCAGCA	62
6	*NKX2.5*	F: CCGCCTTCAAGCCAGAGG R: GAAAGGCAGACGCACACTTG	62
7	*TBXT*	F: TCAAGGCGCACGCTTTCTC R: TTCGTCTCCCTCAGAAGAACCC	62
8	*GATA4*	F: CCTGTCATCTCACTACGGGC R: GTCTGTGGAGACTGGCTGAC	62
9	*MESP1*	F: AGTGAGCGGGAGAAACTGC R: CGACAGGTGGCCGATATAG	62

2.7. Immunofluorescence Cell Imaging

2.7.1. Non-TMEM43 immunofluorescent staining

Cell culture media was removed and the cells were gently washed twice with PBS. Cells were fixed in 10% normal buffered formalin (HT501128, Sigma) for 10 min at room temperature. Following fixation, cells were blocked and permeabilized in 3% BSA + 0.1% Triton X-100 (93426, Sigma) for one hour at room temperature. Samples were incubated in primary antibodies diluted in blocking buffer overnight at 4°C. The following antibodies were used: Rabbit anti-connexin43/CX43 ([1:1000], C6219, Sigma-Aldrich, St. Louis, Missouri, US); mouse anti cardiac troponin T/cTnT ([1:1000], ab8295, Abcam, Cambridge, UK).

Excess primary antibody was washed three times with PBS and samples were incubated in fluorescently-conjugated secondary antibodies and dyes diluted in blocking buffer for one hour at room temperature. The following secondary antibodies and dyes were used: Alexa Fluor 488 donkey anti-rabbit IgG ([1:500], A32731, Invitrogen, Burlington, ON, Canada), Alexa Fluor 555 donkey anti-mouse IgG ([1:500], A32723, Invitrogen) or Alexa Fluor 647 donkey anti-mouse IgG ([1:500], A32787, Invitrogen). Some samples were labelled with Alexa Fluor 555-conjugated phalloidin ([1:500], A34055, Invitrogen) in order to visualize the actin cytoskeleton. Lastly, the nuclear dye Hoechst ([1:1000], H3570, Fisher Scientific) was added and the slide was incubated at room temperature for 5 minutes.

2.7.2. TMEM43 immunofluorescence

Cells were fixed in ice cold methanol (-30°C) for 8 minutes. Samples were washed in PBS and blocked in 3% BSA for one hour at room temperature. Samples were incubated in primary TMEM43 antibody (Rabbit anti TMEM43 ([1:1000], ab230213, Abcam)) diluted in blocking buffer overnight at 4°C. Excess primary antibody was washed three times with PBS and samples were incubated in fluorescently-conjugated secondary antibodies and dyes diluted in blocking buffer for one hour at room temperature. The following secondary antibodies and dyes were used: Alexa Fluor 488 donkey anti-rabbit IgG ([1:500], A32731, Invitrogen). Lastly, Hoechst ([1:1000], H3570, Fisher Scientific) was added and the slide was incubated at room temperature for 5 minutes.

2.7.3. Confocal microscopy

All immunofluorescence staining was performed on a Fluoview FV10i-W3 laser scanning microscope equipped with a 60x water immersion lens (1.2 NA) (system version 2.1.1.7; Olympus, Shinjuku, Tokyo, JP). The following lasers were used to visualize the immunofluorescence stained cells and cellular compartments: 405 nm (Hoechst, DAPI); 473 nm (Alexa Fluor 488, GFP); 559 nm (Alexa Fluor 555); 635 nm (Alexa Fluor 647). Analysis and processing of images were performed by adopting the microscope software and FIJI software (74).

2.8. Calcium imaging

iPSC-CMs were incubated in 5 μM Fluo 4-AM (F14201, Thermo Fisher Scientific) at 37ºC for 30 minutes. Excess Fluo 4-AM was removed and the cells were washed with HEPES balanced salt solution (HBSS, 14025092, Thermo Fisher Scientific). Fresh iPSC-

CM medium (RPMI plus B27) was added to the cells before imaging. Calcium transients of contracting iPSC-CMs (either cell clusters or single cells) was recorded within a given time by confocal laser scanning microscope (Olympus Fluoview FV1000 laser scanning microscope, 20x objective, 458 nm laser, 350 images per 67.8 seconds). After recording calcium sparks of contracting cells without any stimulation, 1µM Isoproterenol (51-30-9, Sigma-Aldrich) was added to the well to record calcium spark after adrenergic receptor stimulation.

2.8.1. Calcium image analysis

Calcium images were analysed in order to calculate the intracellular calcium concentration $[Ca^{2+}]_i$ (68). Images were analysed by means of VS-FlexGrid Pro 8.0J (Olympus) software. The lowest fluorescence transient was considered baseline Fluo4 AM fluorescence intensity when it is not bound to calcium (F_0). The ratio of fluorescent intensity at each time point (F_1) was thus calculated as F_1/F_0. Finally the graph was drawn based on this ratio using GraphPad Prism version 8.0.2 (GraphPad Software Inc, San Diego, US).

2.9. Statistical Analysis

Statistical analysis was performed using GraphPad Prism version 8.0.2 (GraphPad Software Inc, San Diego, US). Data were presented as standard error of the mean (SEM). When three or more samples were compared, one-way analysis of variance (ANOVA) with Tukey's post hoc multiple comparisons test was used to determine statistical significance. In cases where two samples were compared, data was analysed via two-tailed unpaired t-

test. For all experiments, a p-value less than 0.05 was considered significant. *, $p < 0.05$; **, $p < 0.01$; ***, $p < 0.001$; ****, $p < 0.0001$.

3. Results

3.1. TMEM43 protein knockout and life cycle in AD293 reference cells

Some of the most fundamental aspects of TMEM43 protein life cycle are unknown or disputed in the literature. Therefore, our first step was to create and validate a reference *TMEM43* knockout cell line (TMEM43$^{-/-}$) to investigate these fundamental aspects of TMEM43 protein (Figure 5). Two guide RNAs (gRNAs) were designed against the genomic sequence of *TMEM43* using the Sanger CRISPR Finder (http://www.sanger.ac.uk/htgt/wge/find_crisprs) (Figure 5B). Immunofluorescence and Western blot confirm that wild type (WT) human AD293 cells express TMEM43 at the protein level (Figure 5A, C, D). However, after CRISPR-Cas9 gene ablation, TMEM43$^{-/-}$ AD293 cells no longer express TMEM43 protein (Figure 5D). TMEM43$^{-/-}$ AD293 cells appear morphologically similar to control cells (Figure 5C) and we have not observed any major differences in cell growth or survival (data not shown). Therefore, it appears as though TMEM43 is not essential for AD293 cell survival.

Although TMEM43 was first identified nearly 20 years ago (75) the intracellular location of this protein remains controversial (48, 49). Our immunofluorescence staining of cultured AD293 cells revealed the presence of TMEM43 mostly around the nucleus (Figure 5B). TMEM43 knockout cells, on the other hand, show no specific staining. Therefore, TMEM43 appears to indeed be associated with the nuclear envelope in these cells.

Figure 5. TMEM43 localization and CRISPR-Cas9 knockout in human AD293 cells. (A) Immunofluorescence (IF) staining of TMEM43 (green) along with actin (phalloidin, red) and nuclei (DAPI, blue) in wild type AD293 cell line. Scale bar = 10 um. (B) Two guide RNAs were designed targeting the *TMEM43* gene for CRISPR-Cas9 gene ablation in human cells. (C) IF staining of TMEM43 (green) along with nuclei (DAPI, blue) in wild type and TMEM43$^{-/-}$ AD293 cells. Scale bar = 10 um. (D) Western blotting showing TMEM43 expression in control cells which is absent in CRISPR-Cas9 knockout cells.

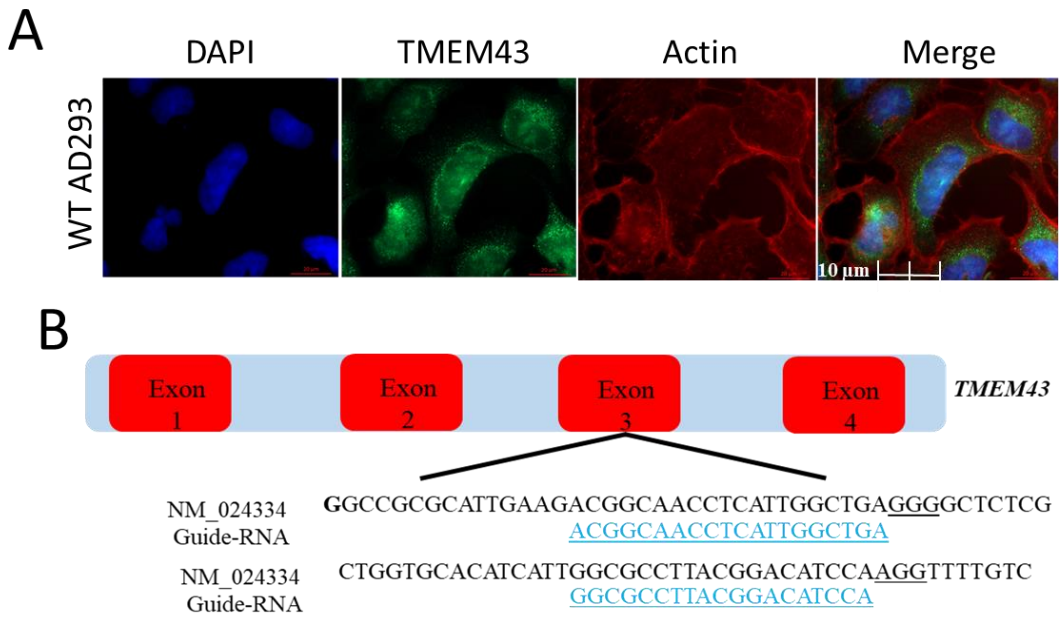
A
DAPI
TMEM43
Actin
Merge
WT AD293
10 µm
B
Exon 1
Exon 2
Exon 3
Exon 4
TMEM43
NM_024334
Guide-RNA
GGCCGCGCATTGAAGACGGCAACCTCATTGGCTGAGGGGCTCTCG
ACGGCAACCTCATTGGCTGA
NM_024334
Guide-RNA
CTGGTGCACATCATTGGCGCCTTACGGACATCCAAGGTTTTGTC
GGCGCCTTACGGACATCCA
C
DAPI
TMEM43
Merge
Wild Type
TMEM43-/-
10 µm
10 µm
D
MW
(kDa)
WT
TMEM43-/-
50 -
TMEM43
37 -
GAPDH

The half-life of a protein can be a key metric to determining how a mutation might affect overall protein function. TMEM43 protein half-life in WT AD293 cells was determined via treatment with cycloheximide (CHX), which suppresses protein synthesis (Figure 6) (76). This assay is used to determine how quickly a protein is naturally degraded in the cell as no new protein can be synthesized during CHX exposure. We were only able to evaluate the cells for up to 8 hours as longer CHX exposure times became cytotoxic to AD293 cells (data not shown). Even after 8 hours of exposure to 25 μM cycloheximide, we found no remarkable decrease in TMEM43 protein expression through Western blotting (Figure 6). On the other hand, Cx43 which has a well-documented half-life of ~1.5 hours exhibited significant protein decrease over the same time period (77). Therefore, these results revealed that wild type TMEM43 is relatively stable with a half-life of more than 8 hours.

3.2. TMEM43 protein knockout and life cycle in human iPSCs

After determining the expression, subcellular localization and half-life of TMEM43 in AD293 cells, we sought to determine whether TMEM43 protein behaves similarly in human iPSCs. Immunofluorescence (IF) and Western blot (WB) demonstrate that wild type (WT) human iPSC cells express TMEM43 at the protein level (Figure 7A, B, C). Generation of TMEM43$^{-/-}$ iPSCs was performed by CRISPR-Cas9 gene ablation using the same CRISPR guide RNAs as the AD293 cells. Immunofluoresence, Western blot and qPCR confirmed the absence of TMEM43 protein in our TMEM43$^{-/-}$ iPSCs (Figure 7B, C, D). TMEM43$^{-/-}$ iPSCs appear morphologically similar to control cells (Figure 7B) and we

Figure 6. Western blot analysis to determine the half-life of TMEM43 in AD293 cells. (A) AD293 cells were treated with either with vehicle control (denoted "0hr") with 25 μM cycloheximide (CHX) for 1, 2, 4 and 8 hours, prior to protein extraction. (B) Relative protein levels of TMEM43 and Cx43, normalized to untreated control. Data represent the standard error of the mean of three independent experiments. NS, no significance; ***, $p < 0.0001$ compared to untreated control as calculated via two-way ANOVA with Tukey's multiple comparisons test.

A

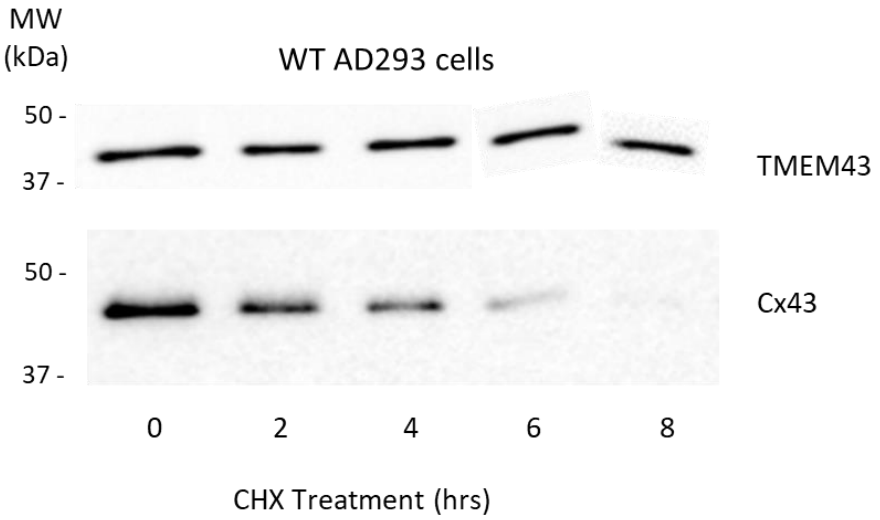
MW
(kDa)
WT AD293 cells
50 -
37 -
TMEM43
50 -
37 -
Cx43
0
2
4
6
8
CHX Treatment (hrs)

B

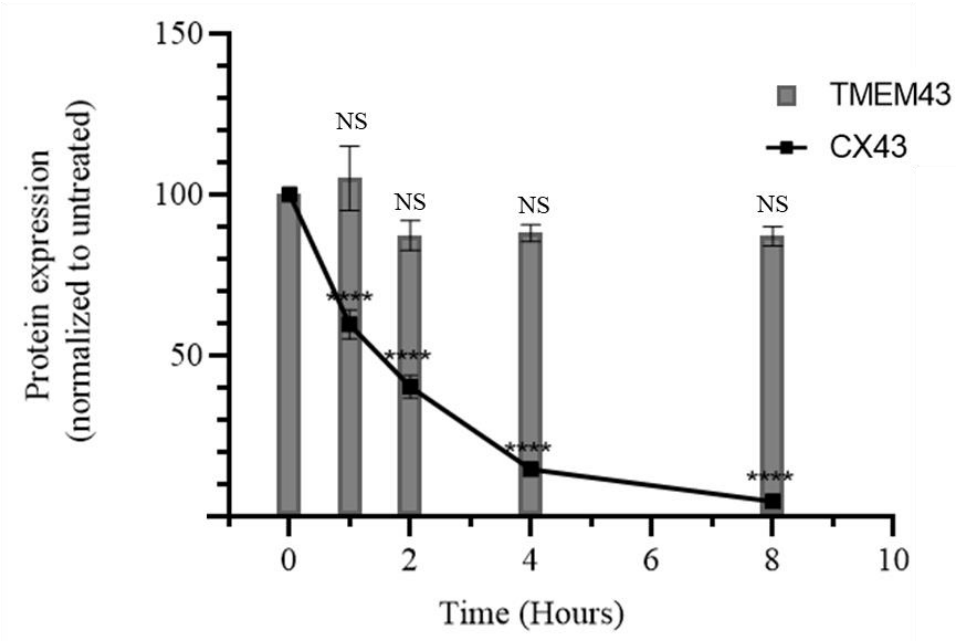
150
100
50
Protein expression
(normalized to untreated)
TMEM43
CX43
NS
NS
NS
NS
****
****
****
****
0
2
4
6
8
10
Time (Hours)

have not observed any major differences in cell growth or survival of undifferentiated iPSCs (data not shown). Therefore, just as TMEM43 was dispensable for AD293 cells, it also appears as though TMEM43 is not essential for iPSCs survival.

3.3. Subcellular localization of TMEM43 protein in human iPSCs.

As described above, we found that TMEM43 was primarily localized to the nuclear envelope of AD293 cells. Interestingly, in contrast with what we observed in human AD293 cells, TMEM43 in iPSCs is not associated with the nuclear envelope; rather TMEM43 exists as large puncta found throughout the cytoplasm (Figure 7B). In order to determine the possible localization of TMEM43 in the other cellular compartments within the cytoplasm we evaluated the co-localization of TMEM43 and calnexin (Endoplasmic reticulum), GM130 (Golgi apparatus), lamin (nuclear envelope) and plakoglobin (desmosomes) (Figure 8). We did not detect any colocalization between TMEM43 and Golgi, nuclear envelope, or desmosomes in wild type iPSCs (8B, C, D). However, there may be partial colocalization of TMEM43 and calnexin which is an ER marker (Figure 8A).

Because we found that TMEM43 localization is vastly different in AD293 cells and iPSCs we hypothesized that the two cell types may exhibit differences in TMEM43 half-life (Figure 9) (81). However, just as we found for the AD293 cells, wild type TMEM43 is also relatively stable in iPSCs with a half-life of more than eight hours (Figure 9).

Figure 7. TMEM43 localization and CRISPR-Cas9 knockout in human female iPSCs. (A) Immunofluorescence staining of TMEM43 (green) along with actin (phalloidin, red) and the nuclei (DAPI, blue). Scale bar = 10µm (B) IF staining (C) Western blotting showing TMEM43 expression in control cells which is absent in CRISPR-Cas9 knockout cells. (D) Quantitative PCR (qPCR) analysis of the relative gene expression level of TMEM43 in WT and TMEM43-KO iPSCs and iPSC-CMs. Data represent the standard error of the mean of 7 independent experiments. ***, $p < 0.001$; ****, $p < 0.0001$ compared to wild type as calculated via one-way ANOVA with Tukey's multiple comparisons test.

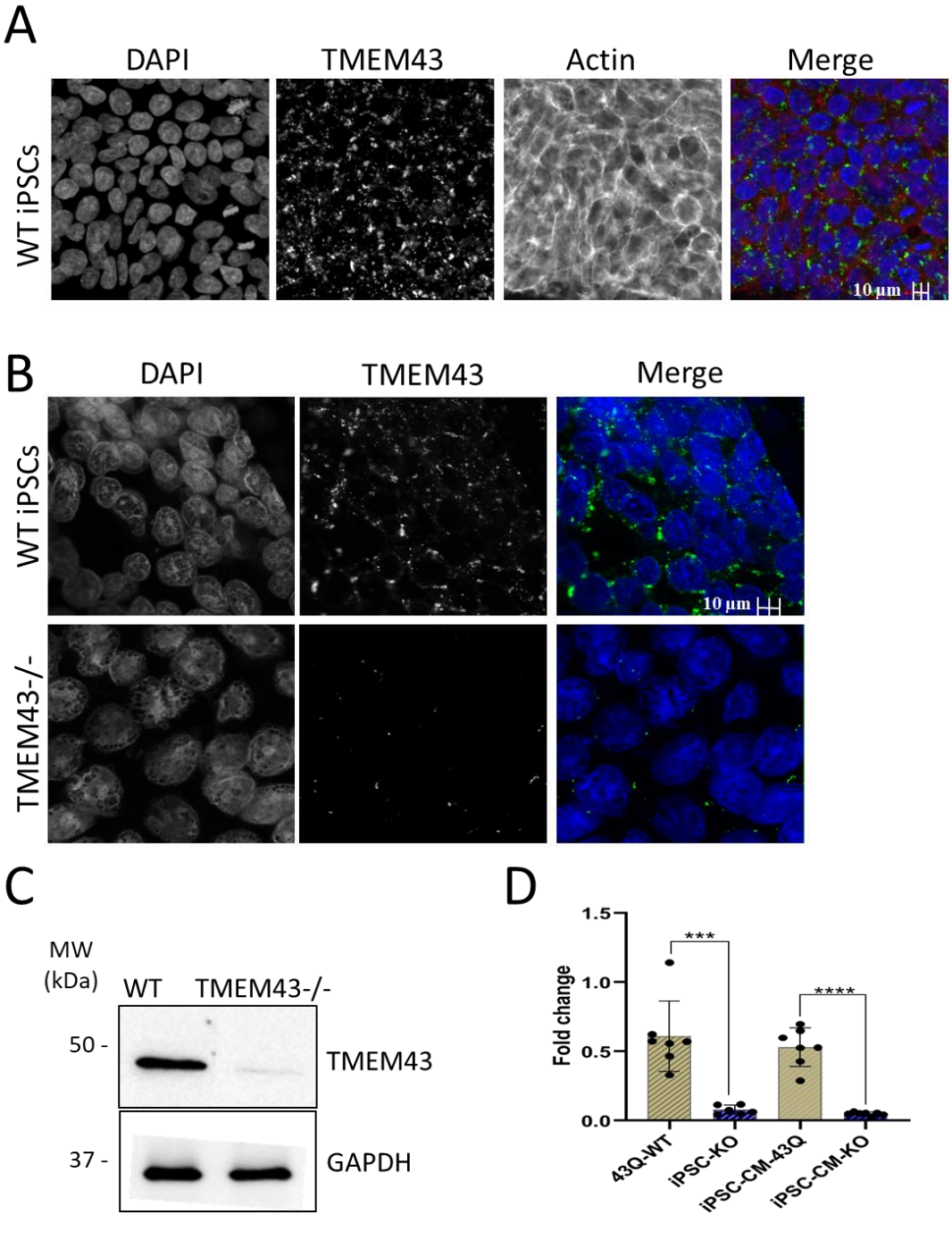
A
DAPI
TMEM43
Actin
Merge
WT iPSCs
10 µm
B
DAPI
TMEM43
Merge
WT iPSCs
10 µm
TMEM43-/-
C
MW
(kDa)
WT
TMEM43-/-
50 -
TMEM43
37 -
GAPDH
D
Fold change
1.5
1.0
0.5
0.0
***
****
43Q-WT
iPSC-KO
iPSC-CM-43Q
iPSC-CM-KO

Figure 8. TMEM43 subcellular distribution in wild type human female iPSCs. Immunofluorescence (IF) staining of TMEM43 (green) along with (A) Calnexin (endoplasmic reticulum, red), (B) GM130 (Golgi apparatus, red), (C) LAMIN (Nuclear Envelope, red), (D) Plakoglobin (desmosomes, red). Nuclei (DAPI, blue). Scale bar = 10μm.

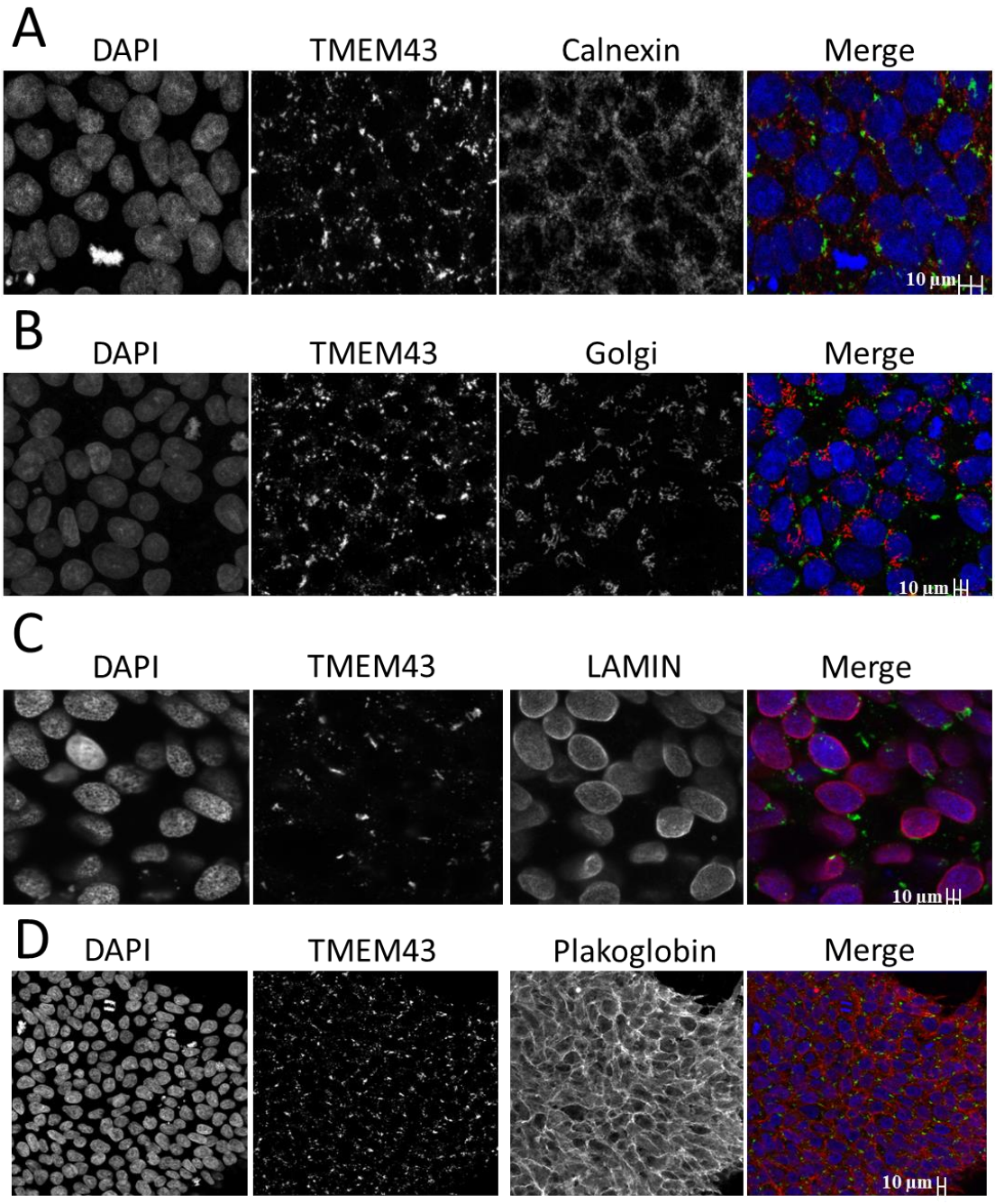
A
DAPI
TMEM43
Calnexin
Merge
10 µm
B
DAPI
TMEM43
Golgi
Merge
10 µm
C
DAPI
TMEM43
LAMIN
Merge
10 µm
D
DAPI
TMEM43
Plakoglobin
Merge
10 µm

Figure 9. Western blot analysis to determine the half-life of TMEM43 in wild type human female iPSCs. (A) Wild type human female iPSCs were treated with 25 μM cycloheximide (CHX) for 0, 1, 2, 4 and 8 hours, prior to protein extraction. Different bands on the Cx43 Western blot show three phosphorylation states of this protein. (B) Relative protein levels of TMEM43 and Cx43, normalized to untreated control. Data represent the standard error of the mean of three independent experiments. NS, no significance; ****, $p < 0.0001$ compared to untreated control as calculated via two-way ANOVA with Tukey's multiple comparisons test.

A

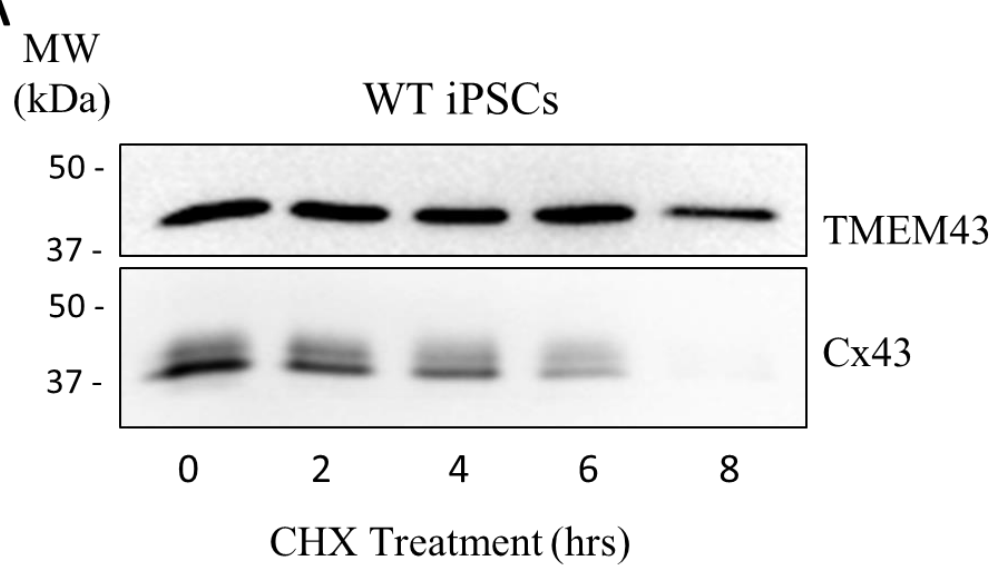
MW
(kDa)
WT iPSCs
50 -
37 -
50 -
37 -
TMEM43
Cx43
0
2
4
6
8
CHX Treatment (hrs)

B

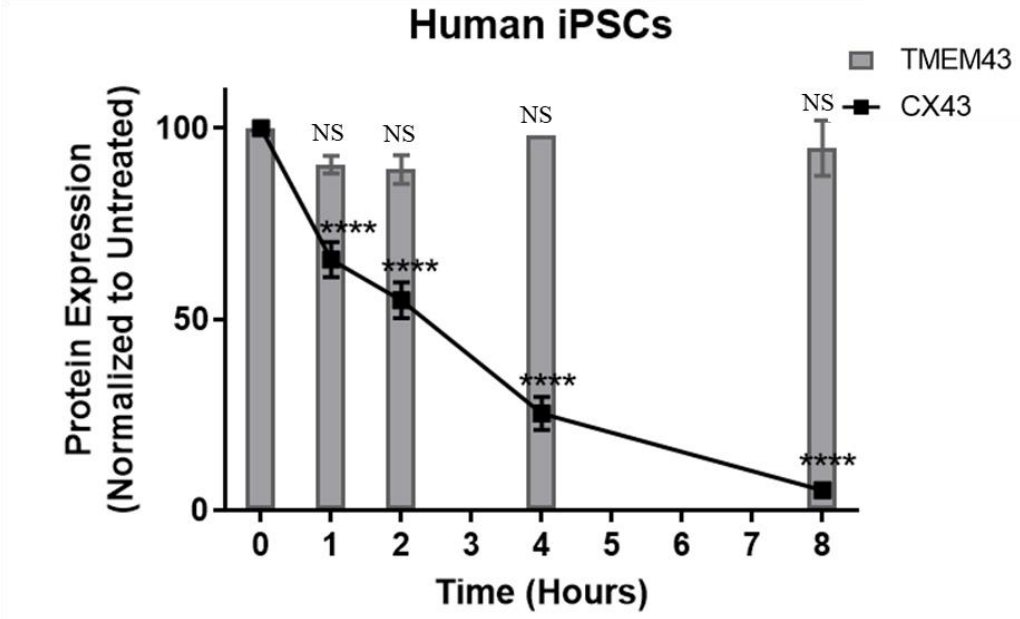
Human iPSCs
TMEM43
CX43
Protein Expression
(Normalized to Untreated)
100
50
0
NS
NS
NS
NS
****
****
****
****
0
1
2
3
4
5
6
7
8
Time (Hours)

3.4. TMEM43 expression in human iPSC-cardiomyocytes

Because ARVC is associated with TMEM43 dysfunction in cardiomyocytes, we next sought to explore TMEM43 expression in human iPSC-derived cardiomyocytes (iPSC-CMs). We investigated both male and female iPSCs to tease out possible sex differences. Differentiated iPSC-CMs begin rhythmically contracting after approximately 14 days in culture and express the appropriate cardiomyocyte markers including *NKX2.5*, *TBX5*, *GATA-4* and *TNNT* (Figure 10B-G). Indeed, qPCR demonstrates significant upregulation of each of these key cardiac genes in iPSC-derived cardiomyocytes compared to undifferentiated iPSCs (Figure 10B-G). IF staining of iPSC-CMs also showed the presence of cardiac troponin T (Figure 11A) and Cx43 (Figure 11B) in contracting cells. The IF staining of TMEM43 revealed the localization pattern of this protein within iPSC-CM (Figure 11C).

Spontaneously contracting iPSC-derived cardiomyocytes also exhibit rhythmic calcium release and reuptake as demonstrated by the fluorescent calcium binding dye Fluo4-AM (Figure 12A, B, D). Peak frequency, duration and amplitude were constant and regular, indicating normal function in regulating intracellular calcium transients during rhythmic contraction. However, we have noted that different contracting clusters of WT iPSC-CMs can exhibit different contraction frequencies and peak calcium amplitudes (Figure 12A, B). Finally, adrenergic receptor stimulation with isoproterenol increases the contraction-related calcium transients in control iPSC-CMs (Figure 12C).

Figure 10. Characterization of wild type human female IPSC-derived cardiomyocytes. (A) Phase contrast image of a region of contracting iPSC-CMs. Scale bar = 10μm (B) Densitometric analysis and (C) representative Western blot indicating that iPSC-derived Cardiomyocytes upregulate cardiac troponin T protein (TNNT) compared to undifferentiated iPSCs. (D-G) Quantitative reverse-transcribed polymerase chain reaction (qPCR) analysis demonstrated increased expression of the cardiac-specific genes (D) NKX2.5, (E) TBX1, (F) GATA4 and (G) TNNT. Data represent the standard error of the mean of 4-9 experiments. *, $p < 0.05$; ** $p<0.01$ compared to undifferentiated iPSCs as analyzed via unpaired, two way t-test.

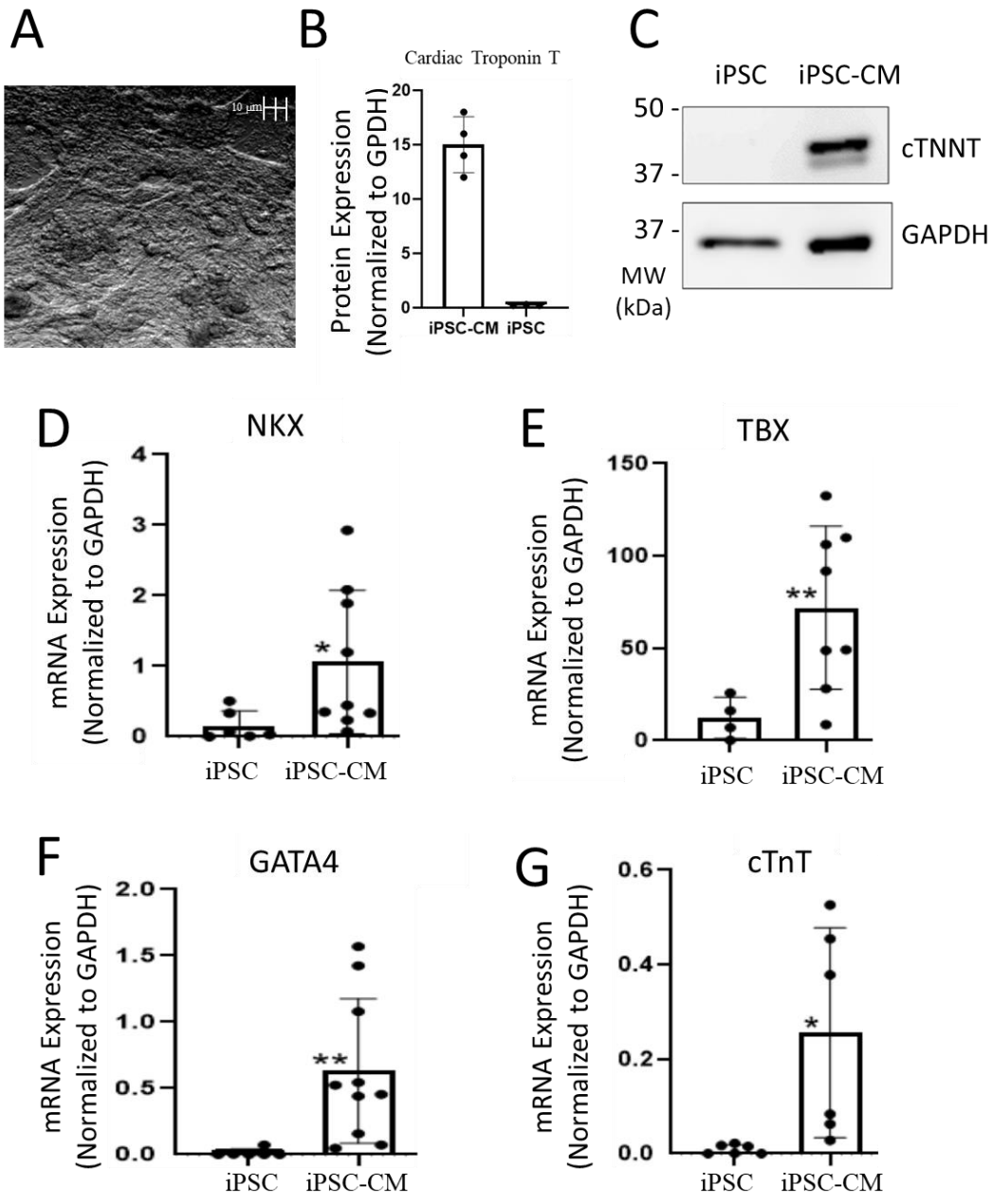
A
10 μm
B
Cardiac Troponin T
Protein Expression (Normalized to GPDH)
20
15
10
5
0
iPSC-CM iPSC
C
iPSC iPSC-CM
50
37
37
MW (kDa)
cTNNT
GAPDH
D
NKX
mRNA Expression (Normalized to GAPDH)
4
3
2
1
0
*
iPSC iPSC-CM
E
TBX
mRNA Expression (Normalized to GAPDH)
150
100
50
0
**
iPSC iPSC-CM
F
GATA4
mRNA Expression (Normalized to GAPDH)
2.0
1.5
1.0
0.5
0.0
**
iPSC iPSC-CM
G
cTnT
mRNA Expression (Normalized to GAPDH)
0.6
0.4
0.2
0.0
*
iPSC iPSC-CM

Figure 11. Wild type human female iPSC-CMs express TMEM43 and cardiomyocyte markers. (A) IF staining of TMEM43 (green) along with the nuclei (DAPI, blue) in iPSC-derived cardiomyocytes. (B) Cx43 (green) and nuclei (DAPI, blue) in iPSC-CMs. (C) cTnT (red) and nuclei (DAPI, blue) in iPSC-CM. Scale bar = 10µm.

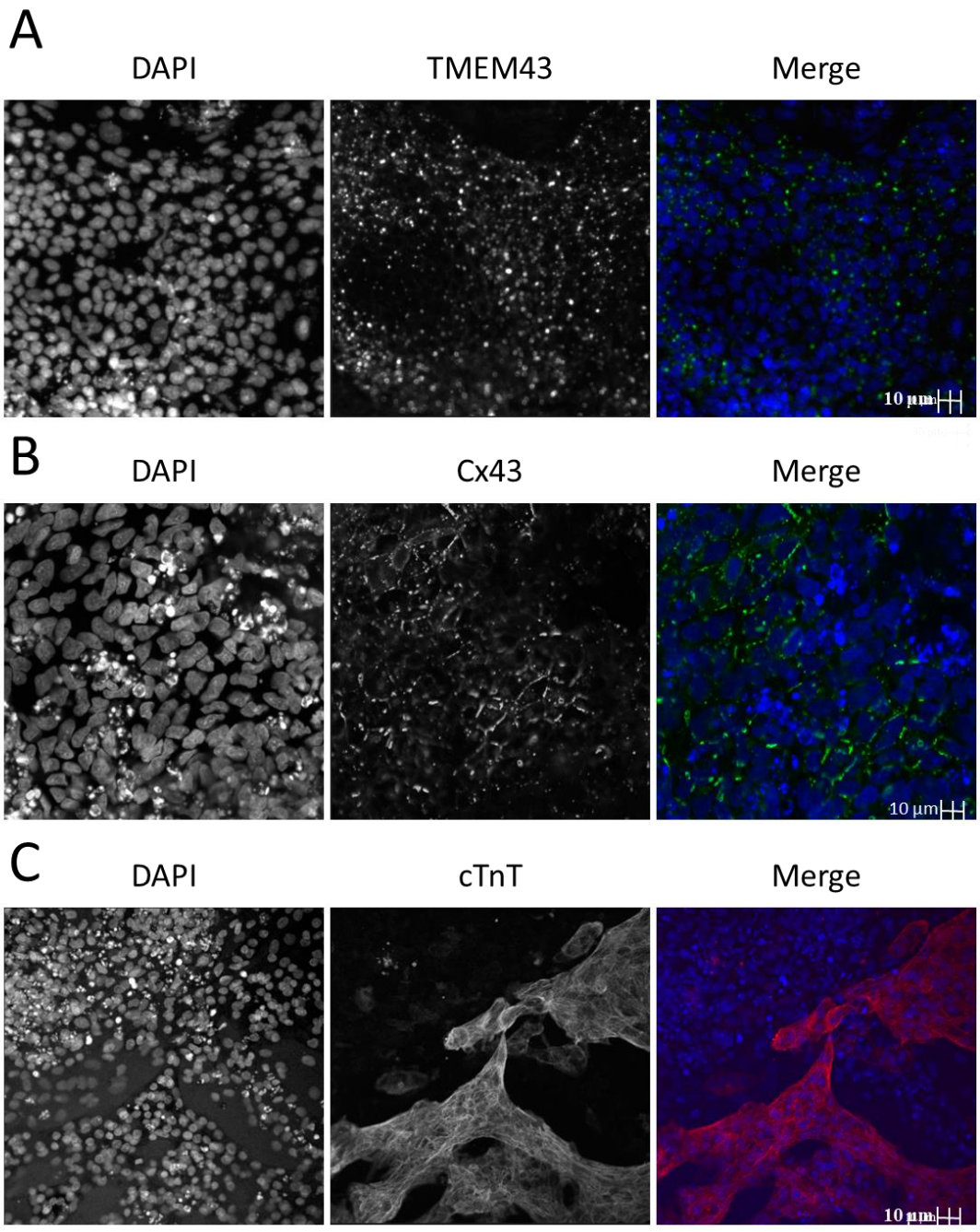
A
DAPI
TMEM43
Merge
10 µm
B
DAPI
Cx43
Merge
10 µm
C
DAPI
cTnT
Merge
10 µm

Figure 12. Cyclic calcium release in wild type female iPSC-derived cardiomyocytes. (A) Line-scan image of Ca^{2+} transients and the average fluorescence intensity in two independent spontaneously contracting female wild type iPSC-CM cell clusters. (B) Intracellular calcium concentration within spontaneous contraction of iPSC-CMs. (C) Wild type iPSC-CM contraction rate after adding 1 μM isoproterenol. (D) Calcium imaging of single cell of iPSC-CM after adding 0.5 mM $CaCl_2$ to stimulate the cells for contraction.

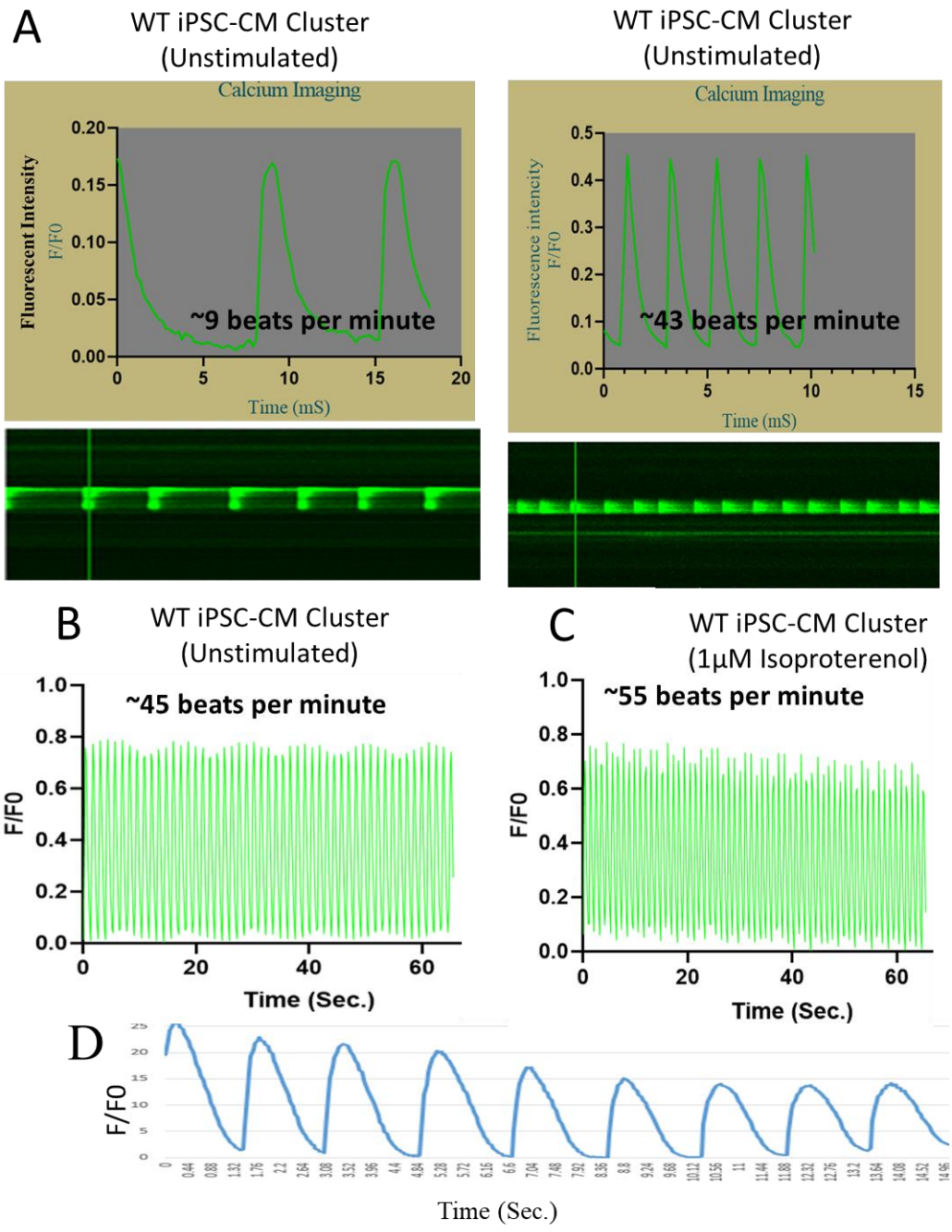
A
WT iPSC-CM Cluster
(Unstimulated)
Calcium Imaging
Fluorescent Intensity
F/F0
~9 beats per minute
Time (mS)
WT iPSC-CM Cluster
(Unstimulated)
Calcium Imaging
Fluorescence intencity
F/F0
~43 beats per minute
Time (mS)
B
WT iPSC-CM Cluster
(Unstimulated)
~45 beats per minute
F/F0
Time (Sec.)
C
WT iPSC-CM Cluster
(1µM Isoproterenol)
~55 beats per minute
F/F0
Time (Sec.)
D
F/F0
Time (Sec.)

When evaluating female iPSCs, qPCR and Western blot revealed that TMEM43 was expressed at approximately equal amounts in iPSCs as well as iPSC-derived cardiomyocytes (Figure 13A, B, E). The gap junction protein Cx43 was also similarly expressed between iPSCs and iPSC-CMs (Figure 13C, D). In contrast to female iPSCs, male iPSCs upregulated TMEM43 after differentiation into cardiomyocytes (Figure 13E). Interestingly, when comparing male and female iPSCs or iPSC-CMs, we found significant difference in the expression of TMEM43 and Cx43 between male and female cells (Figure 13E, F).

Figure 13. Sex differences between cardiomyocytes derived from male and female iPSCs. (A) Representative Western blot and (B) densitometric analysis of TMEM43 protein expression in female iPSCs and iPSC-CMs. (C) Representative Western blot and (D) densitometric analysis of Cx43 protein expression in female iPSCs and iPSC-CMs. (E) Relative TMEM43 mRNA expression in male and female iPSCs and iPSC-CMs. (F) Relative Cx43 mRNA expression level in male and female iPSCs and iPSC-CMs. Data represent the standard error of the mean of 3-4 independent experiments. Ns, not significant; **, $p < 0.01$; ***, $p < 0.001$ compared to female iPSCs.

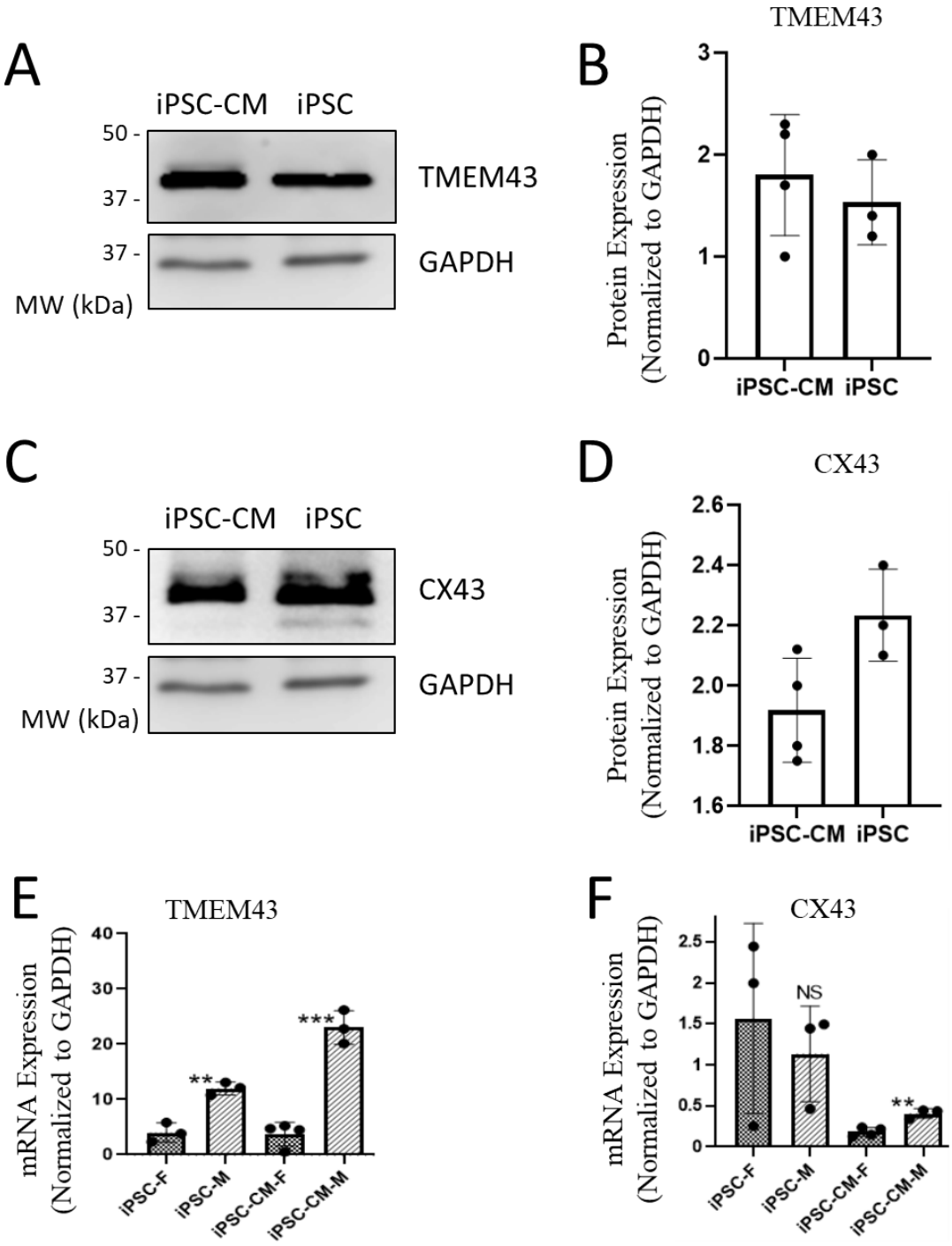
A
iPSC-CM
iPSC
50 -
37 -
37 -
MW (kDa)
TMEM43
GAPDH
B
TMEM43
Protein Expression
(Normalized to GAPDH)
3
2
1
0
iPSC-CM
iPSC
C
iPSC-CM
iPSC
50 -
37 -
37 -
MW (kDa)
CX43
GAPDH
D
CX43
Protein Expression
(Normalized to GAPDH)
2.6
2.4
2.2
2.0
1.8
1.6
iPSC-CM
iPSC
E
TMEM43
mRNA Expression
(Normalized to GAPDH)
40
30
20
10
0
**
***
iPSC-F
iPSC-M
iPSC-CM-F
iPSC-CM-M
F
CX43
mRNA Expression
(Normalized to GAPDH)
2.5
2
1.5
1
0.5
0
NS
**
iPSC-F
iPSC-M
iPSC-CM-F
iPSC-CM-M

4. Discussion

4.1. Arrhythmogenic Right Ventricular Cardiomyopathy (ARVC)

ARVC is a category of life-threatening diseases characterized by fibrofatty replacement of heart tissue, particularly throughout the RV. Cardiac arrhythmias, SCD, heart remodelling and dilated cardiomyopathy are all hallmarks of these disorders (16, 34). Ventricular tachycardia with a LBBB pattern as well as epsilon wave due to fibro-fatty replacement of the RV free wall was reported in ARVC-affected individuals (42). ARVC symptoms such as palpation and SCD can be observed after childhood (18). Heart enlargement and inverted T wave are also two of the most common signs in this disease (42).

The inheritable and particularly pathological ARVC type 5 is caused by an autosomal dominant mutation in the *TMEM43* gene and is widely prevalent throughout Newfoundland (52). Although many other types of ARVC are caused by mutations in desmosomal genes, ARVC5 is due to mutation in the non-desmosomal gene *TMEM43*. Regardless, the signs and symptoms of ARVC5 are consistent with other types of ARVC, including cardiac arrhythmias leading to SCD, cardiomyopathy leading to end stage heart failure and sex differences between male and female patients (22, 52).

4.2. TMEM43 expression and localization in different cells and tissues

In 2008, Bengtsson and Otto examined TMEM43 mRNA expression across different human tissues. TMEM43 was highly expressed in the placenta, testis and prostate while the heart, skeletal muscle and liver expressed lower amounts of this protein (49). Conversely, TMEM43 was reported to be abundantly expressed throughout the mouse lung,

spleen and heart (50). It remains to be determined whether these contrasting findings are related to species differences, age of the tissue or pathological disease state. We find that TMEM43 is expressed at similar levels in AD293 cells and iPSCs (Figure 5 and 13). Interestingly, while we found that female iPSC and iPSC-CMs expressed approximately equal levels of TMEM43, male cells significantly upregulated TMEM43 after differentiation (Figure 13). Both AD293 cells and iPSCs stem from epithelial cells which may account for the similar levels of TMEM43 expression. However, we also noted that female iPSC-derived cardiomyocytes express similar TMEM43 transcript and protein levels to AD293 cells and iPSCs. As cardiomyocytes are mesenchymal in nature, cell lineage may not entirely account for gene expression.

TMEM43 is reported to interact with several nucleoskeleton proteins including emerin and lamin (53, 80). *In silico* investigations showed that TMEM43 contains four transmembrane domains (TMD) with a large hydrophilic loop (49). Immunofluorescent labelling has placed TMEM43 to the nuclear envelope of several human and mouse cell lines including HeLa, NIH 3T3, 293T and C2C12 cells (49, 53). TMEM43 reportedly fails to localize to the inner nuclear membrane (INM) of mouse embryonic fibroblasts that lack A-type lamins ($LMNA^{-/-}$ MEFs) suggesting that TMEM43 interaction with lamin type A is essential to ensure proper TMEM43 localization (49). TMEM43 has also been localized to the nuclear envelope in human and mouse cardiac tissue and fibroblasts (50). Electron microscopy suggests that the hydrophilic loop projects from the outer nuclear membrane into the endoplasmic reticulum (51).

In addition to the nuclear envelope, TMEM43 has been shown to localize to the endoplasmic reticulum in several model systems (52, 51) as well as the intercalated disc and gap junctions (48, 49, 51). Therefore, TMEM43 may be alternatively trafficked in different cell or tissue types. It is possible that this altered trafficking patterns may impact the function of TMEM43 throughout the body. Moreover, TMEM43 mutation may alter the protein trafficking which may contribute to the pathology. TMEM43-S358L overexpression constructs have been suggested to aggregate in phagosomes within the cells due to defunct protein oligomerization (51).

In the current research we examined the expression of wild type TMEM43 in three different human cell types including AD293, iPSC and iPSC-CM. Western blot analysis indicates that all of these cells express similar levels of TMEM43 (Figure 5 and 13), however, it appears to be differentially localized across the different cell types. As has been reported by others, we found that TMEM43 was primarily localized around the nuclear envelope of AD293 cells (Figure 5). Interestingly, we find TMEM43 is not localized within the nuclear envelope of human iPSCs; rather TMEM43 in iPSCs exists as a puncta throughout the cytoplasm (Figure 7, 8). Furthermore, this localization pattern persists for iPSC derived cardiomyocyte (Figure 11), which conflicts with previously published reports showing TMEM43 around the nuclear envelope in human and mouse heart tissue (51, 56). The immature nature of our iPSC-CMs may account for these discrepancies. In order to determine specifically which subcellular compartment TMEM43 is localized to in human iPSCs, we performed immunofluorescence staining for TMEM43 along with markers for the Golgi apparatus (GM130), endoplasmic reticulum (calnexin), nuclear envelope (Lamin)

and desmosomes (Plakoglobin) (Figure 8). We find very little evidence that TMEM43 in iPSCs is located within the Golgi, nuclear envelope or desmosomes. However, TMEM43 may be partially colocalized with the ER (Figure 8) which has been shown in other cell types (54). Recently, one of my labmates discovered that the intracellular TMEM43 puncta in iPSCs co-localize with the early endosome marker EEA1. It remains to be determined how TMEM43 is trafficked to early endosomes in iPSCs, or what function it may serve there.

4.3. TMEM43 protein half-life

TMEM43 is a conserved protein which is found in vertebrates, insects, bacteria and plants (78). TMEM43 is a 400 amino acid protein with the mass of ~44.8 kDa. In order to improve our understanding about the life cycle of TMEM43, we determined the half-life of TMEM43. We found that the half-life of TMEM43 is longer than eight hours in both AD293 cells and iPSCs (Figures 6, 9). It remains to be seen whether TMEM43 mutation affects the stability of the protein. Determining the half-life of the mutant protein may shed light on the mechanism of pathogenesis. If, for example, it is determined that mutant TMEM43 also has a long half-life, then the mutant protein may negatively impact the function of the wild type isoform. On the other hand, if the mutant protein is more unstable and has a shorter half-life, it may lead to haploinsufficiency as the cell would not have enough protein for normal function. Either way, understanding the basic life cycle of the wild type and mutant forms of this protein is essential to uncovering the molecular mechanisms of ARVC.

4.4. iPSC-derived cardiomyocytes as a model of cardiomyocyte function

As outlined in section 1.5.4, animal models have failed to recapitulate key aspects of ARVC pathology (56). Therefore, in this study we sought to find a more human-oriented model in which to study these cellular and molecular processes. Human iPSC-derived cardiomyocytes are easily accessible and amenable to manipulation (70, 79). There are also well-established methods for differentiating human iPSCs into contracting cardiomyocytes (70). Our iPSC-derived cardiomyocytes expressed appropriate cardiomyocyte markers including cardiac troponin T (Figure 10G, 11C) and connexin43 (Figure 11B, 13D, F) and GATA4 (Figure 10F). We found that the expression level of TMEM43 is similar in undifferentiated iPSCs and iPSC-derived cardiomyocytes. Furthermore, our wild type iPSC-CMs showed normal, constant and regular contraction and cycled calcium (Figure 12). However, we found that wild type cells exhibit differences in contraction frequency and calcium release even within the same dish (Figure 12A). In response to adrenergic receptor stimulation with isoproterenol, wild type iPSC-CMs increase contraction frequency and show enhanced calcium release (Figure 12B, C). Thus iPSC-CM has many advantages as a cell model for heart disease investigation.

4.6. ARVC5 pathology is sex-dependent

As with other forms of ARVC, TMEM43-associated ARVC type 5 is much more severe in males compared to females (52). Because of this, we sought to determine whether male and female iPSCs and iPSC-CMs exhibit differences in TMEM43 expression. We found that TMEM43 and the gap junction protein Cx43 were expressed at approximately equal amounts in iPSCs as well as iPSC-CMs. Interestingly, male (XY) iPSCs express

significantly higher levels of TMEM43 compared to female (XX) iPSCs. Moreover, male cells significantly upregulated TMEM43 after differentiation into cardiomyocytes, while female iPSCs do not (Figure 13). In addition to being isolated from donors of different sex, these cells are also from individuals of divergent ethnic backgrounds. Therefore, these findings must be validated on ARVC patient samples, as well as samples from individuals from similar ethnic backgrounds. However, if our results are found to be true in these circumstances, increased expression of TMEM43 mutation in males may exert a more profound effect on men versus women. Additionally, it is necessary to determine whether other cell types (in addition to cardiomyocytes) also follow the pattern of being more highly expressed in male samples.

4.7. Study Limitations

As discussed in the introduction, a major limitation to the use of iPSC-derived cardiomyocytes is the maturity and purity of the resulting culture. The differentiation protocol that we have employed, as is the case with most other protocols, generates primarily immature cardiomyocytes, reminiscent of fetal cells (67). Therefore, these cells lack key attributes of mature cardiomyocytes. For example, although adult ventricular cardiomyocytes are contractile cells, they are not able to contract spontaneously, while our iPSC-CMs are able to spontaneously contract. Unlike adult cardiomyocytes, our calcium imaging demonstrates that iPSC-CMs lack a plateau phase and instead there is a rapid decrease in calcium spark (Figure 12A). Finally, we also find inherent differences in contraction frequency and calcium release in iPSC-derived cardiomyocytes. Therefore, caution is necessary when critically evaluating results comparing different cell lines.

However, many researchers around the world are working to mature iPSC-derived cardiomyocytes in culture. Recently, it has been demonstrated that cardiac fibroblasts, and cardiac endothelial cells are effective in maturation of iPSC-CM. This strategy for maturation can improve the sarcomeric structures with T-tubules in iPSC-CM and enhance the contraction feature of these cells (80).

5. Conclusions

In this study we uncover some of the most fundamental properties of the TMEM43 protein. Our data demonstrate that wild type TMEM43 has a half-life of more than eight hours in examined human cells. We found that TMEM43 is differentially localized in human AD293 cells and human iPSCs, and we were able to successfully knockout TMEM43 in these cells using CRISPR-Cas9. TMEM43$^{-/-}$ AD293 cells and iPSCs appear morphologically similar to control cells and we noticed no appreciable difference in survival and growth of cells. Thus, it appears as though TMEM43 is not essential for human AD293 cell or iPSC survival or proliferation.

We used human iPSC-CMs as a model to uncover the cellular and molecular functions of wild type TMEM43 in cardiomyocytes. Gene expression analysis combined with morphology, contractile ability and associated calcium handling of iPSC-CMs confirmed that we had successfully differentiated cardiomyocytes from iPSCs.

6. Perspectives and future directions

Heart failure and particularly SCD are the disastrous consequence of TMEM43-associated ARVC5. Unfortunately, there is currently no cure for this disease. Efforts to

understand ARVC5 are hampered by the lack of information about the molecular role of TMEM43 protein and the impact of TMEM43 mutation at the cellular level. The work presented here represents a starting point for a long-term research project to be continued after I finish. I have designed and validated two human TMEM43 CRISPR-Cas9 guide RNAs and we have female TMEM43$^{-/-}$ iPSCs in-house. Because ARVC is more severe in men than women, it will be important to also generate TMEM43$^{-/-}$ male iPSCs. Once these knockout cells are in-hand they can be evaluated for cardiomyocyte contraction, Ca^{2+} transients, desmosome and gap junction expression, and apoptosis. These studies will reveal how complete TMEM43 loss affects human cardiomyocyte function. The ultimate goal of this project is to model ARVC5 using patient-derived iPSCs. With ARVC5 iPSCs we can uncover the half-life of mutant TMEM43 in iPSC-CMs, how heterozygous TMEM43 mutation affects the wild type allele and other interacting proteins, how male and female patient samples differ, as well as the multiple facets of cardiomyocyte function as we have described here.

7. References

1- Sherwood L, Ward C. Human physiology: from cells to systems. 3th ed. Belmont, CA: Brooks/Cole, Cengage Learning; 2016:295-303.

2- Litviňuková M, Talavera-López C, Maatz H. et al. Cells of the adult human heart. *Nature*. 2020. doi.org/10.1038/s41586-020-2797-4.

3- Eisner DA, Caldwell JL, Kistamás K, Trafford AW. Calcium and Excitation-Contraction Coupling in the Heart. *Circ Res.* 2017;121(2):181-195. doi:10.1161/CIRCRESAHA.117.310230.

4- Brade T, Pane LS, Moretti A, Chien KR, Laugwitz KL. Embryonic heart progenitors and cardiogenesis. *Cold Spring Harb Perspect Med.* 2013;3(10):a013847-55. doi:10.1101/cshperspect.a013847.

5- Garry DJ, Olson EN. A common progenitor at the heart of development. *Cell*. 2006;127(6):1101-4. doi:10.1016/j.cell.2006.11.031.

6- Saga Y, Kitajima S, Miyagawa-Tomita S. Mesp1 expression is the earliest sign of cardiovascular development. *Trends Cardiovasc Med*. 2000;10(8):345-52. doi:10.1016/s1050-1738(01)00069-x.

7- Olson EN. Sizing up the heart: development redux in disease. *Genes Dev*. 2003;17(16):1937-1956. doi:10.1101/gad.1110103.

8- Rajala K, Pekkanen-Mattila M, Aalto-Setälä K. Cardiac differentiation of pluripotent stem cells. *Stem Cells Int*. 2011;2011:383709. doi:10.4061/2011/383709.

9- Anderson DJ, Kaplan DI, Bell KM, et al. NKX2-5 regulates human cardiomyogenesis via a HEY2 dependent transcriptional network. *Nat Commun*. 2018;9(1):1373. doi:10.1038/s41467-018-03714-x

10- Ma L, Sun B, Hood L, Tian Q. Molecular profiling of stem cells. *Clin Chim Acta.* 2007;378(1-2):24-32. doi:10.1016/j.cca.2006.12.016.

11- Reiser PJ. Current understanding of conventional and novel co-expression patterns of mammalian sarcomeric myosin heavy chains and light chains. *Arch Biochem Biophys*. 2019;662: 129-133. doi:10.1016/j.abb.2018.12.009.

12- Scuderi GJ, Butcher J. Naturally Engineered Maturation of Cardiomyocytes. *Front Cell Dev Biol.*2017;5:50-5. doi:10.3389/fcell.2017.00050.

13- Soonpaa MH, Kim KK, Pajak L, Franklin M, Field LJ. Cardiomyocyte DNA synthesis and binucleation during murine development. *Am J Physiol.* 1996;271(5):H2183-H2189. doi:10.1152/ajpheart.1996.271.5.H2183.

14- Mezzano V, Pellman J, Sheikh F. Cell junctions in the specialized conduction system of the heart. *Cell Commun Adhes*. 2014;21(3):149-159. doi:10.3109/15419061.2014.905928.

15- Davis LM, Rodefeld ME, Green K, Beyer EC, Saffitz JE. Gap junction protein phenotypes of the human heart and conduction system [published correction appears in J Cardiovasc Electrophysiol 1996 Apr;7(4):383-5]. *J Cardiovasc Electrophysiol*. 1995;6(10 Pt 1):813-822. doi:10.1111/j.1540-8167.1995.tb00357.x

16- Gandjbakhch E, Redheuil A, Pousset F, Charron P, Frank R. Clinical Diagnosis, Imaging, and Genetics of Arrhythmogenic Right Ventricular Cardiomyopathy/Dysplasia: JACC State-of-the-Art Review. *J Am Coll Cardiol*. 2018;72(7):784-804. doi:10.1016/j.jacc.2018.05.065.

17- Mezzano V, Sheikh F. Cell-cell junction remodeling in the heart: possible role in cardiac conduction system function and arrhythmias? *Life Sci*. 2012;90(9-10):313-321. doi:10.1016/j.lfs.2011.12.009.

18- Kottke MD, Delva E and Kowalczyk AP. The desmosome: cell science lessons from human diseases. *J Cell Sci*. 2006;119(Pt 5):797-806. doi:10.1242/jcs.02888.

19- Tariq H, Bella J, Jowitt TA, et al. Cadherin flexibility provides a key difference between desmosomes and adherens junctions. *Proc Natl Acad Sci USA*. 2015;112(17):5395-5400. doi:10.1073/pnas.1420508112

20- Garcia-Gras E, Lombardi R, Giocondo MJ, et al. Suppression of canonical Wnt/beta-catenin signaling by nuclear plakoglobin recapitulates phenotype of arrhythmogenic right ventricular cardiomyopathy. *J Clin Invest.* 2006;116(7):2012-2021. doi:10.1172/JCI27751.

21- Sattar Y, Abdullah HM, Neisani Samani E, Myla M, Ullah W. Arrhythmogenic Right Ventricular Cardiomyopathy/Dysplasia: An Updated Review of Diagnosis and Management. *Cureus*. 2019;11(8):e5381. Published 2019 Aug 13. doi:10.7759/cureus.5381

22- Corrado D, Link MS, Calkins H. Arrhythmogenic Right Ventricular Cardiomyopathy. *N Engl J Med*. 2017; 376(1):61-72. doi:10.1056/NEJMra1509267.

23- Austin KM, Trembley MA, Chandler SF, et al. Molecular mechanisms of arrhythmogenic cardiomyopathy. *Nat Rev Cardiol*. 2019;16(9):519-537. doi:10.1038/s41569-019-0200-7.

24- Statistics Canada, Catalogue no. HP35-85/1-2018E. Ottawa.

https://www.canada.ca/en/public-health/services/publications/diseases-conditions/report-heart-disease-Canada-2018.html. Published May 2018.

Accessed May 15, 2020.

25- Schoen FJ, Mitchell RN. The Heart. In: Kumar V, ed. Robbins and Cotran pathologic basis of disease. 9th ed. Philadelphia, PA: Elsevier/Saunders; 2005: 551-568.

26- Breitenstein A, Steffel J. Devices in Heart Failure Patients—Who Benefits From ICD and CRT? *Front Cardiovasc Med*. 2019;6:111. doi:10.3389/fcvm.2019.00111

27- Longo DL, Fauci A, Kasper D, Hauser S, Jameson JL, Loscalzo J. Harrisons manual of medicine. 18th ed. New York: Mcgraw-hill Education - Europe. 2016:823-829.

28- Brieler J, Breeden MA, Tucker J. Cardiomyopathy: An Overview. *Am Fam Physician*. 2017;96(10):640-646.

29- Lakdawala NK, Winterfield JR, Funke BH. Dilated cardiomyopathy. *Circ Arrhythm Electrophysiol*. 2013;6(1):228-237. doi:10.1161/CIRCEP.111.962050.

30- Marcus FI, Zareba W, Calkins H, et al. Arrhythmogenic right ventricular cardiomyopathy/dysplasia clinical presentation and diagnostic evaluation: results from the North American Multidisciplinary *Study. Heart Rhythm*. 2009;6(7):984-992. doi:10.1016/j.hrthm.2009.03.013.

31- Maron BJ, Towbin JA, Thiene G, et al. Contemporary definitions and classification of the cardiomyopathies: an American Heart Association Scientific Statement from the Council on Clinical Cardiology, Heart Failure and Transplantation Committee; Quality of Care and Outcomes Research and Functional Genomics and Translational Biology Interdisciplinary Working Groups; and Council on Epidemiology and Prevention. *Circ.*2006;113(14):1807-16. doi:10.1161/CIRCULATIONAHA.106.174287.

32- Thiene G, Nava A, Corrado D, Rossi L, Pennelli N. Right ventricular cardiomyopathy and sudden death in young people. *N Engl J Med*. 1988; 318(3):129-33. doi:10.1056/NEJM198801213180301.

33- Basso C, Thiene G, Corrado D. Arrhythmogenic right ventricular cardiomyopathy: dysplasia, dystrophy, or myocarditis? *Circ*.1996;94(5):983-91. doi:10.1161/01.cir.94.5.983.

34- Marcus FI, Fontaine GH, Guiraudon G, et al. Right ventricular dysplasia: a report of 24 adult cases. *Circ*.1982;65(2):384-98. doi:10.1161/01.cir.65.2.384.

35- Garcia-Gras E, Lombardi R, Giocondo MJ, et al. Suppression of canonical Wnt/beta-catenin signaling by nuclear plakoglobin recapitulates phenotype of arrhythmogenic right ventricular cardiomyopathy. *J Clin Invest*. 2006;116(7):2012-2021. doi:10.1172/JCI27751.

36- Weippert M, Behrens K, Rieger A, Stoll R, Kreuzfeld S. Heart rate variability and blood pressure during dynamic and static exercise at similar heart rate levels. *PLoS One.* 2013;8(12):e83690. Published 2013 Dec 13. doi:10.1371/journal.pone.0083690.

37- Prichard BN1, Owens CW, Smith CC, Walden RJ. Heart and catecholamines. *Acta Cardiol*. 1991;46(3):309-22.

38- Lefkowitz RJ, Rockman HA, Koch WJ. Catecholamines, Cardiac β-Adrenergic Receptors, and Heart Failure. *Circ*. 2000;101(14):1634-7. doi:10.1161/01.CIR.101.14.1634.

39- Bhagat BD, Rao PS, Dhalla NS. Role of catecholamines in the genesis of arrhythmias. *Adv Myocardiol.* 1980;2:117-32.

40- Schömig A, Haass M, Richardt G. Catecholamine release and arrhythmias in acute myocardial ischaemia. *Eur Heart J.* 1991;12 Suppl F:38-47. doi:10.1093/eurheartj/12.suppl_f.38.

41- Yoerger DM, Marcus F, Sherrill D, et al. Echocardiographic findings in patients meeting task force criteria for arrhythmogenic right ventricular dysplasia: new insights from the Multidisciplinary Study of Right Ventricular Dysplasia. *J Am Coll Cardiol*.2005;45(6):860-5. doi:10.1016/j.jacc.2004.10.070.

42- Marcus FI, McKenna WJ, Sherrill D, et al. Diagnosis of arrhythmogenic right ventricular cardiomyopathy/dysplasia: proposed modification of the Task Force Criteria. *Eur Heart J.* 2010;31(7):806-814. doi:10.1093/eurheartj/ehq025.

43- Delmar M, Liang FX. Connexin43 and the regulation of intercalated disc function. *Heart Rhythm.* 2012;9(5):835-838. doi:10.1016/j.hrthm.2011.10.028.

44- Sato PY, Musa H, Coombs W, et al. Loss of plakophilin-2 expression leads to decreased sodium current and slower conduction velocity in cultured cardiac myocytes. *Circ Re*s. 2009;105(6):523-526. doi:10.1161/CIRCRESAHA.109.201418.

45- Herren T, Gerber PA, Duru F. Arrhythmogenic right ventricular cardiomyopathy/ dysplasia: a not so rare "disease of the desmosome" with multiple clinical presentations. *Clin Res Cardiol*. 2009;98(3):141-58. doi:10.1007/s00392-009-0751-4.

46- Asimaki A, Saffitz JE. The role of endomyocardial biopsy in ARVC: looking beyond histology in search of new diagnostic markers. *J Cardiovasc Electrophysiol*. 2011;22(1):111-117. doi:10.1111/j.1540-8167.2010.01960.x

47- Schirmer EC, Foisner R. Proteins that associate with lamins: many faces, many functions. *Exp Cell Res*. 2007;313(10):2167-79. doi:10.1016/j.yexcr.2007.03.012.

48- Stroud MJ. Linker of nucleoskeleton and cytoskeleton complex proteins in cardiomyopathy. *Biophys Rev*. 2018;10(4):1033-1051. doi:10.1007/s12551-018-0431-6.

49- Bengtsson L, Otto H. LUMA interacts with emerin and influences its distribution at the inner nuclear membrane. *J Cell Sci.* 2008;121(Pt 4):536-48. doi:10.1242/jcs.019281.

50- Stroud MJ, Fang X, Zhang J, et al. Luma is not essential for murine cardiac development and function. *Cardiovasc Res*. 2018;114(3):378-388. doi:10.1093/cvr/cvx205.

51- Siragam V, Cui X, Masse S, et al. TMEM43 mutation p.S358L alters intercalated disc protein expression and reduces conduction velocity in arrhythmogenic right ventricular cardiomyopathy. *PLoS One*. 2014;9(10):e109128. doi:10.1371/journal.pone.0109128.

52- Merner ND, Hodgkinson KA, Haywood AF, et al. Arrhythmogenic right ventricular cardiomyopathy type 5 is a fully penetrant, lethal arrhythmic disorder caused by a missense mutation in the TMEM43 gene. *Am J Hum Genet*. 2008;82(4):809-821. doi:10.1016/j.ajhg .2008.01.010.

53- Milting H, Klauke B, Christensen AH, et al. The TMEM43 Newfoundland mutation p.S358L causing ARVC-5 was imported from Europe and increases the stiffness of the cell nucleus. *Eur Heart J*. 2015;36(14):872-81. doi: 10.1093/eurheartj/ehu077

54- Christensen AH, Andersen CB, Tybjaerg-Hansen A, et al. Mutation analysis and evaluation of the cardiac localization of TMEM43 in arrhythmogenic right ventricular cardiomyopathy. *Clin Genet*. 2011;80(3):256-64. doi:10.1111/j.1399-0004.2011.01623.

55- Baskin B, Skinner JR, Sanatani S, et al. TMEM43 mutations associated with arrhythmogenic right ventricular cardiomyopathy in non-Newfoundland populations. *Hum Genet.* 2013;132(11):1245–1252. doi:10.1007/s00439-013-1323-2.

56- Padrón-Barthe L, Villalba-Orero M, Gómez-Salinero JM, et al. Severe Cardiac Dysfunction and Death Caused by Arrhythmogenic Right Ventricular Cardiomyopathy Type 5 Are Improved by Inhibition of Glycogen Synthase Kinase-3β. *Circulation*. 2019;140(14):1188-1204. doi:10.1161/CIRCULATIONAHA.119.040366.

57- Meyer T, Sartipy P, Blind F, Leisgen C, Guenther E. New cell models and assays in cardiac safety profiling. *Expert Opin Drug Metab Toxicol*. 2007;3(4):507-17. doi:10.1517/17425225.3.4.507.

58- Kehat I, Kenyagin-Karsenti D, Snir M, et al. Human embryonic stem cells can differentiate into myocytes with structural and functional properties of cardiomyocytes. *J Clin Invest*. 2001;108(3):407-414. doi:10.1172/JCI12131.

59- Takahashi K, Yamanaka S. Induction of pluripotent stem cells from mouse embryonic and adult fibroblast cultures by defined factors. *Cell*. 2006; 126(4): 663–76. doi: 10.1016/j.cell.2006.07.024.

60- Zakrzewski W, Dobrzyński M, Szymonowicz M, Rybak Z. Stem cells: past, present, and future. *Stem Cell Res Ther*. 2019;10(1):68-75. doi:10.1186/s13287-019-1165-5.

61- Loh YH, Wu Q, Chew JL, et al. The Oct4 and Nanog transcription network regulates pluripotency in mouse embryonic stem cells. *Nat Genet.* 2006;38(4):431-40.

62- He JQ, Ma Y, Lee Y, Thomson JA, Kamp TJ. Human embryonic stem cells develop into multiple types of cardiac myocytes: action potential characterization. *Circ Res*. 2003 11;93(1):32-9. doi: 10.1161/01.RES.0000080317.92718.99.

63- Mummery C, Ward-van Oostwaard D, Doevendans P, et al. Differentiation of human embryonic stem cells to cardiomyocytes: role of coculture with visceral endoderm-like cells. *Circ*. 2003;107(21):2733–2740. doi:10.1161/01.CIR.0000068356.38592.68.

64- Chen VC, Stull R, Joo D, Cheng X, Keller G. Notch signaling respecifies the hemangioblast to a cardiac fate. *Nat Biotechnol*. 2008;26(10):1169-1178. doi:10.1038/nbt.1497.

65- Tseng AIS, Engel FB, Keating M. The GSK-3 inhibitor BIO promotes proliferation in mammalian cardiomyocytes. *Chem Biol.* 2006;13(9):957–963. doi:10.1016/j.chembiol.2006.08.004.

66- McDevitt TC, Laflamme MA, Murry CE. Proliferation of cardiomyocytes derived from human embryonic stem cells is mediated via the IGF/PI 3-kinase/Akt signaling pathway. *J Mol Cell Cardiol.* 2005;39(6):865-873. doi:10.1016/j.yjmcc.2005.09.007.

67- Karbassi E, Fenix A, Marchiano S, et al. Cardiomyocyte maturation: advances in knowledge and implications for regenerative medicine. *Nat Rev Cardiol*. 2020;17(6):341-359. doi:10.1038/s41569-019-0331-x

68- Guatimosim S, Guatimosim C, Song LS. Imaging calcium sparks in cardiac myocytes. *Methods Mol Biol*. 2011;689:205-214. doi:10.1007/978-1-60761-950-5_12.

69- Esseltine JL, Shao Q, Brooks C, et al. 2017. Connexin43 Mutant Patient-Derived Induced Pluripotent Stem Cells Exhibit Altered Differentiation Potential. *J Bone Miner Res*. 2017;32(6): 1368–1385. doi:10.1002/jbmr.3098

70- Chen G, Gulbranson DR, Hou Z, et al. Chemically defined conditions for human iPSC derivation and culture. *Nat Methods*. 2011;8(5):424–429. doi:10.1038/nmeth.1593.

71- Esseltine JL, Brooks CR, Edwards NA, et al. Dynamic regulation of connexins in stem cell pluripotency. *Stem Cells.* 2020;38(1):52-66. doi: 10.1002/stem.3092.

72- Shao Q, Esseltine JL, Huang T, et al. Connexin43 is Dispensable for Early Stage Human Mesenchymal Stem Cell Adipogenic Differentiation But is Protective against Cell Senescence. *Biomol*. 2019;9(9):474. doi:10.3390/biom9090474.

73- Ran FA, Hsu PD, Wright J, Agarwala V, Scott DA, Zhang F. Genome engineering using the CRISPR-Cas9 system. *Nat Protoc*. 2013;8(11):2281–2308. doi:10.1038/nprot.2013.143.

74- Schindelin J, Arganda-Carreras I, Frise E, et al. Fiji: an open-source platform for biological-image analysis. Nat Methods 2012;9:676–682. doi.org/10.1038/nmeth.

75- Dreger M, Bengtsson L, Schöneberg T, Otto H, Hucho F. Nuclear envelope proteomics: novel integral membrane proteins of the inner nuclear membrane. *Proc Natl Acad Sci USA*. 2001; 98(21):11943-11948. doi:10.1073/pnas.211201898.

76- Watanabe-Asano T, Kuma A, Mizushima N. Cycloheximide inhibits starvation-induced autophagy through mTORC1 activation. *Biochem Biophys Res Commun.* 2014;445(2):334-9. doi:10.1016/j.bbrc.2014.01.180.

77- Beardslee MA, Laing JG, Beyer EC, Saffitz JE. Rapid Turnover of Connexin43 in the Adult Rat Heart. *Circ Res.* 1998;83:629–635. doi:10.1161/01.RES.83.6.629.

78- Mans BJ, Anantharaman V, Aravind L, Koonin EV. Comparative genomics, evolution and origins of the nuclear envelope and nuclear pore complex. *Cell Cycle*. 2004;3(12):1612-37. doi:10.4161/cc.3.12.1345.

79- Matsa E, Burridge PW, Wu JC. Human stem cells for modeling heart disease and for drug discovery. *Sci Transl Med*. 2014;6(239):239ps6. doi:10.1126/scitranslmed.3008921

80- Giacomelli E, Meraviglia V, Campostrini G, et al. Human-iPSC-Derived Cardiac Stromal Cells Enhance Maturation in 3D Cardiac Microtissues and Reveal Non cardiomyocyte Contributions to Heart Disease. *Cell Stem Cell*. 2020;26(6):862-879.e11. doi:10.1016/j.stem.2020.05.004.

8. Appendix A

Protease-activated receptor-2 regulates myocardial ischemic injury through AMPK

By Hooman Sadighian

Master of Science in Medicine (Cardiology & Renal Physiology)

Division of BioMedical Sciences/Faculty of Medicine

Memorial University of Newfoundland

2018-2019

St. John's, Newfoundland and Labrador, Canada

Supervisor: Dr. Dake Qi

Abstract

The rupture of atherosclerotic plaques leading to obstruct blood flow to the heart is the principal cause of myocardial infarction (MI). The inadequate blood supply thus disrupts cardiomyocyte ATP generation leading to cardiomyocyte death. AMP-activated protein kinase (AMPK), playing a key role in cellular energy regulation, can have an important part in reducing reperfusion injury in the post-ischemic phase of MI. Protease-activated receptor-2 (PAR2), identified in endothelial cells, has been reported to regulate AMPK activity, however there remains a lack of information about the potential role PAR2 may play in adult cardiomyocytes. Thus, our current study investigates the role of PAR2 in mediating AMPK and downstream signaling molecules in isolated adult rat cardiomyocytes. PAR2 expression in adult rat cardiomyocytes was confirmed via qPCR. Pharmacological activation of PAR2 in isolated cardiomyocytes significantly reduced AMPK phosphorylation, and increased the active form of acetyl-coA carboxylase 1, suggesting a role in fatty acid synthesis.

Table of Contents

List of Figures

List of Tables

A.1. Introduction

Myocardial infarction (MI) is one of the major causes of mortality and morbidity in Canada and worldwide. Occlusion of coronary arteries due to formation and rupture of an atherosclerotic plaque is the leading cause of MI (1, 2). Coronary artery plaque formation leads to ischemia (lack of blood flow), in which the heart is not adequately supplied with oxygen and nutrients. Following ischemia, blood vessel reperfusion once again allows oxygen and nutrients to reach the damage area. However, this can also lead to ischemia/reperfusion (I/R) injury (1, 2). Therefore, there is a large push for therapies to mitigate myocardial damage due to lack of oxygen and nutrients.

Given the incredible demands put upon the heart, it is not surprising that this organ has vast energy requirements. The main sources of energy for the heart are fatty acids and glucose. The regulation of glucose catabolism and FA β-oxidation is necessary for appropriate cardiac activity. 5' AMP-activated protein kinase (AMPK) plays an essential role in regulating cell metabolism both through increased ATP generation and decreased ATP consumption. Thus, AMPK activity results in the activation of β-oxidation pathway as well as increasing the uptake of glucose (3). Intracellular AMPK plays principal role in energy homeostasis of cell. The high level of intracellular ATP leads to inactivation of AMPK or generation of unphosphorylated AMPK (16, 17, 18). Regulation of lipid metabolism is one the function of this molecule. AMPK activation upregulate fatty acid metabolism and inhibits fatty acid synthesis. AMPK inhibits FA synthesis through the phosphorylation of acetyl-coA carboxylase 1 (pACC1) which is inactive form of this molecule (19, 20). ACC is involved in fatty acid synthesis by converting acetyl-coA to

malonyl-coA playing role in fatty acid synthesis. Thus, AMPK can lead to inhibitory phosphorylation of ACC and consequently increases FA β-oxidation and production of ATP from FA (21, 22).

PAR-2 is a member of the seven transmembrane protease activated receptor (PAR) family. PAR receptors feature an extracellular amino-terminus that can activate the receptor through protease cleavage. Protease cleavage of the amino-terminus generates a type of tethered ligand that can activate the receptor (4). Like other members of the G protein coupled-receptor superfamily, PAR activation triggers exchange of GTP for GDP on the associated heterotrimeric G protein and subsequent signal transduction cascade. PAR-2 may be an attractive candidate to regulate AMPK in order to decease the I/R injury within the MI (5).

The PAR2 receptor is a seven transmembrane domain G protein coupled receptor (4, 13, 14, 15). This receptor was reported to express in various cells and several animal models. It has negative effect in some of the tissues, however, beneficial effect of PAR2 was reported in the other disease such as airway inflammation and ischemic brain injury. Activation of endothelial PAR2 has a vasodilator effect on coronary vessels. PAR2 has also been shown to exhibit inflammatory effect in some diseases (4). While PAR2 expression has been confirmed in human, mouse and rat heart, as well as rat neonatal cardiomyocytes, it remains unclear whether this receptor is expressed in isolated adult rat cardiomyocytes and the possible impact of this receptor on infarct size.

A1.1. Research questions:

1- Is PAR-2 expressed in isolated adult rat ventricular cardiomyocytes?

2- Does PAR2 activation regulate AMPK phosphorylation?

3- Does PAR2 activation regulate ACC phosphorylation?

A2. Material and Methods

A2.1. Adult rat ventricular cardiomyocyte isolation

All studies were approved by the Memorial University of Newfoundland Animal Care Committee (protocol # 16-02-DQ). Sprague Dawley IGS rats were used in this study (Charles River, Crl:CD (SD)). Cardiomyocytes, heart tissue and aorta tissue were obtained from 10 adult rats aged 50 to 80 days. Two animals were housed together were free fed normal rat chow and water.

Several factors affect the quality of isolated adult cardiomyocytes. These factors include quality of water, clean and disinfected glass-wares, pH and temperature of employed solutions, quality and concentration of chemical compounds such as collagenase and avoiding the formation of air bubble during heart perfusion (6, 7). Adult rat heart dissociation was performed using the Langendorff apparatus accompanied with circulation of enzymatic perfusate through aorta and left ventricle (Figure A1). The cannula was 1.6 mm in diameter and was adjustable with the size of aorta. The perfusate was maintained at 37°C. A drip chamber was utilized in Langendorff apparatus to avoid circulation of bubbles in perfusate (6, 7).

A2.1.1. Animal preparation

Intraperitoneal (IP) injection of heparin (400–5000 u/kg B.W.) was performed 30 minutes before dissection of heart. Subsequently, IP injection of pentobarbital (Sodium pentobarbital 40 -60 mg/kg IP) was carried out for anesthesia (6, 8). About 5 minutes after

pentobarbital injection animal response to pinch was evaluated. Heart dissection occurred only once the rat was adequately heparinized and anesthetized.

A2.1.2. Heart dissection and cannulation:

The chest cavity of the anaesthetized rat was opened to have full access to the heart. The heart and attached intact aortic arch were rapidly excised and immersed in a cold Joklik solution (buffer composition in Table A1). Excess tissue around the heart and aorta were removed using forceps and scissors. It is necessary to keep aorta intact to use it for heart cannulating. The aorta was placed over the cannula, and fixed into position by tying silk suture thread around the aorta (Figure A1) (6, 8).

Figure A1. Isolation of adult rat ventricular cardiomyocyte apparatus. After heart dissection, the heart is positioned on cannula by aorta and the pump circulates the perfusate (8ml/min) including oxygenated Joklik. Collagenase solution was circulated (8ml/min) to digest the heart tissue. After almost 30 minutes of digestion, the heart tissue is ready for dissociation and cardiomyocyte purification. A drip chamber is located in this circuit to capture any possible bubbles. Water bath is adjusted to maintain the temperature of circulated perfusate at 37°C.

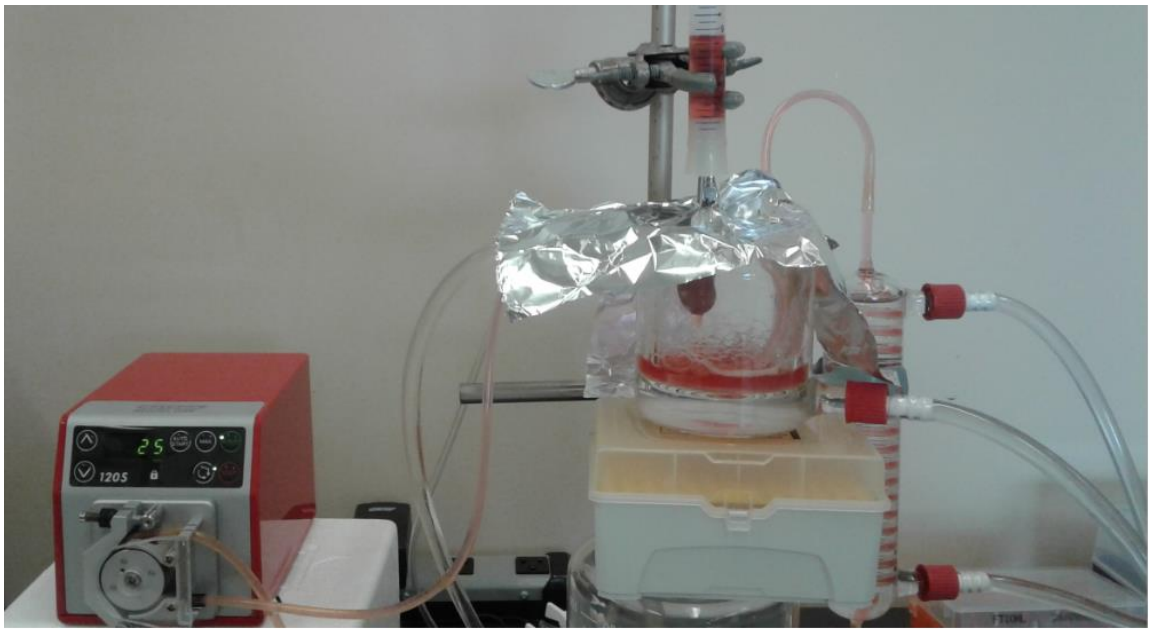

Rat Heart Dissection	Rat Cannulation	Cardiac perfusion	Enzymatic digestion	Cardiomyocyte purification

A2.1.3. Digestion of heart

Once the Joklik solution was circulated throughout the cannulated heart, collagenase solution was added (buffer composition in Table A2) in order to digest the heart tissue gradually, and dissociate cardiomyocytes. The circulation of collagenase generally takes approximately 40 minutes. After collagenase digestion, the left ventricle is dissected using sterile forceps in a petri dish. The circulated collagenase solution was added to heart tissue and the entire solution filtered with a 70μm pore to isolate single cells (22-363-548, Thermofisher Scientific, Waltham, Massachusetts, US). Collected filtered cell suspension was centrifuged in 300 x g for 2 minutes at room temperature to concentrate isolated cardiomyocytes (6, 7, 8).

C1 solution (buffer composition in Table A2) was added to the pellet. The cell suspension was oxygenated and incubated at 37°C in water bath for ten minutes. Then the supernatant was removed and C2 solution (buffer composition in Table A2) was added to the cell pellet for 10 minutes, followed by C3 solution (buffer composition in Table A2). The final cell suspension was plated onto a laminin coated dish. In order to prepare laminated dish, 4% of laminin (L2020, Sigma-Aldrich) is diluted in M199 medium (11150059, Thermofisher Scientific, Waltham, Massachusetts, US). Isolated cardiomyocytes are cultured in M199 plus medium (Table A3) in a humidified 37°C cell culture incubator with 5% CO2 (6, 8).

PAR2 pharmacological activation in extracted cardiomyocytes was conducted by adding 30 nM of the PAR2 activator (2-Furoyl-LIGRLO-amide trifluoroacetate salt) (2fli,

F3681, Sigma-Aldrich) (9, 10, 11). PAR2 antagonist GB83 (10 μM) (Sigma-Aldrich,) was used to prevent and block the PAR2 activation (9, 10, 12).

Table A1. Joklik Solution

Distilled water	900 ml	
Jaklik powder (Minimum Essential Medium Eagle)	11.23 g	(56419C , Sigma-Aldrich, St. Louis, Missouri, United States)
Sodium bicarbonate	2 g (23 mM)	(S5761, Sigma-Aldrich)
Magnesium sulfate	0.144 g (1.2 mM)	(M7506, Sigma-Aldrich)
L-Carnitine hydrochloride	0.198 g (1 mM)	(C0283, Sigma-Aldrich)
pH	7.4	

Filter-sterilize and store in 4°C. This solution should be oxygenated for 30 minutes prior to use.

Table A2. Solutions for the isolation of cardiomyocyte

Solution	Joklik	BSA (A2153, Sigma-Aldrich)	Calcium Chloride (1M, C1016, Sigma-Aldrich)	Collagenase type II (C6885, Sigma-Aldrich)
C1	50 ml	0.5	100 µl (0.1 mM)	-
C2	50 ml	0.5	250µl (0.25 mM)	-
C3	50 ml	0.5	500µl (0.5 mM)	-
Collagenase	50 ml	0.5	12.5µl (0.0125 mM)	50 mg

Table A3. M199 plus medium

M199 medium	100ml
HEPES	0.595 g
L-Carnitin (C0283, Sigma-Aldrich)	0.02 g
PS solution (Streptomycin + Penicillin) (15140122, Thermofisher Scientific, Waltham, Massachusetts, US)	1 ml (Streptomycin 0.01 g + Penicillin 0.01g)

A2.2. Western Blotting

A2.2.1- Extraction of proteins from cell culture

Cell culture media was discarded and the cells were washed twice with ice-cold phosphate buffered saline solution (PBS, 140 mM NaCl (600-082-DG, Wisent), 2.6 mM KCl (P330-500, Fisher Scientific), 1.4 mM KH_2PO_4 (BP362500, Fisher Scientific)). PBS was discarded and ice-cold lysis buffer was added (150 mM NaCl; 1.0% Triton X-100; 50 mM Tris pH 8.0). After 10 minutes incubation at 4°C, the cells were collected with cold plastic cell scraper and transferred to the microcentrifuge tube. Lysates were centrifuged at 14000 x g for 10 minutes at 4°C to pellet the insoluble material. The supernatant as cell lysate was kept at -20°C until further use.

A2.2.2. Protein assay

Protein concentration was determined in duplicate using the Pierce BCA Protein Assay Kit (PI23225, Thermo Scientific) according to the manufacturer's instructions. Colorimetric detection was performed on a VICTOR plate reader (model 2030, Perkin Elmer, Waltham, Massachusetts, US) at 595nm light. Protein concentrations were extrapolated using a bovine serum albumin (BSA; B4287, Sigma, MO, USA) standard curve of known protein concentrations (Standard curve from 0-4 µg/ml). Protein concentration was interpolated from the BSA standard curve using the formula $y = mx + b$, where m is the slope, b is the y-intercept and x is the unknown protein concentration.

A2.2.3. SDS-PAGE

Proteins were separated via sodium dodecyl sulfate polyacrylamide gel electrophoresis (SDS-PAGE). For each sample, 20 µg protein were loaded into each well and the volume of every single sample was brought to 20 µl, using PBS. Protein denaturation and loading buffer (10% SDS, 50% Glycerol, 0.5% Bromophenol Blue, 250 mM Tris-HCl, pH 6.8, and, add 5% 2-mercaptoethanol) was added to each sample prior to separation via SDS-PAGE. After that samples were mixed well and placed at boiling water bath for 10 minutes. Protein samples were loaded into a 7.5% poly-acrylamide gel (EC-890, National Diagnostics, Atlanta, Georgia, US) and run at 100 volt using the Mini Trans-Blot® Cell (1658005, Biorad, CA, USA). The gel was transferred to the nitrocellulose membrane (0.45 µm pore size, 1620115, Bio Rad) at 100 volt for an hour at 4°C.

A2.2.4. Immunoblotting

The membrane was blocked with 3% non-fat milk (Carnation®) for 1 hour at room temperature, then incubated with primary antibody diluted in a 3% instant skim milk powder in Tris Buffered Saline with Tween 20 (TBS-T) (15.2 mM Tris HCL, 46.2 mM Tris base (1610719, Bio Rad), 150.6 mM NaCl (600-082-DG, Wisent), and 0.1% Tween 20 (BP337100, Fisher BioReagents)) overnight at 4°C. The following primary antibodies were used: Rabbit anti pAMPK ([1:1000], 2531S, cell signal, Danvers, Massachusetts, USA); Rabbit anti- Total AMPK ([1:1000], 5832S, cell signal, Danvers, Massachusetts, USA). Excess primary antibody was washed from the membrane with TBS-T (3 washes of 10 minutes each) and membranes were incubated with horseradish peroxidase (HRP)-labeled secondary antibody diluted in 5% BSA solution in TBS-T for one hour at room temperature. The following secondary antibodies were used: horse anti mouse-HRP

([1:1000], 7076S, cell signal, Danvers, Massachusetts, USA) and goat anti rabbit-HRP ([1:1000], 7074S, cell signal, Danvers, Massachusetts, USA). Excess secondary antibody was washed from the membrane with TBS-T (3 washes of 10 minutes each) and exposed using ECL (1705061, Bio Rad). Blots were visualized using the Image Quant LAS 4000 series (28 9558 10, GE Healthcare, Chicago, Illinois, US).

A2.2.5. Immunoblot analysis

Western blots were analyzed by densitometry using FIJI software (79). The integrated density of each sample was calculated by FIJI.

A2.3. Quantitative Real-time PCR (qRT-PCR)

A2.3.1. RNA extraction

Total RNA of cardiomyocytes were extracted by TRIZOL (15596026, Thermo Scientific). Extracted RNA was kept in -80°C. The quantity and quality of extracted RNA of each sample was measured by nanodrop (NanoDrop™ 2000/2000c Spectrophotometers, ThermoFisher Scientific). High quality RNA is assessed as having a λ260/280 ratio of ~2.0 and a λ260/230 ratio of ~2.2. 500 ng of extracted RNA was used to generate cDNA by using the High-Capacity cDNA Reverse Transcription Kit (4387406, Thermo Scientific). cDNA was stored at -20°C until use.

A2.3.2. Quantitative Reverse Transcription Polymerase Chain Reaction (qPCR)

Gene expression was assessed via quantitative qPCR using SYBR green (1725124, Bio-rad). Primer sequences are outlined in (Table A4). The reference gene was *GAPDH* while target gene was PAR2. qPCR was performed in Applied Biosystems 7500 Real-Time PCR

thermocycler (Applied Biosystems, USA). Cycle conditions were as follows: pre denaturation 95°C, 5 minutes, initial denaturation 95°C, 15 seconds, primer annealing/extension 60°C, 60 seconds, 40 cycle. The melting curves of amplicons were gained with temperatures ranging from 50°C to 95°C with a 0.05°C increase in temperature every second. Values were normalized to aorta. Three technical replicates were included across each of ten biological replicates.

A2.4. Statistical Analysis

Statistical analysis was performed using GraphPad Prism version 8.0.2 (GraphPad Software Inc, San Diego, US). Data were presented as standard error of the mean (SEM) values. One-way analysis of variance (ANOVA) with Tukey's post-hoc multiple comparisons test was used to determine statistical significance for qPCR outcomes. T-test (two-tailed) was used for Western blotting results. For all experiments, a p-value less than 0.05 was considered significant.

Table A4. Primer sequences for qPCR

	Name	Sequence (5′ to 3′)	Annealing Temp (°C)
1	*Gapdh*	F: GACAGTCAGCCGCATCTTCT R: GCGCCCAATACGACCAAATC	60
2	*Par2*	F: CTGACTTTCTCTCGGTGCGT R: GGGGTTCACGATGACCCAAT	60

A3. Results

A3.1. Adult rat ventricular cardiomyocytes express PAR2.

We initially identified if PAR-2 is expressed in adult rat ventricular cardiomyocytes. The adult rat cardiomyocytes were isolated and cultured (M199 plus) for 48 hours. These cells were then collected to extract the protein and RNA. Aorta and intact adult rat heart tissues were used to positive control. Consistent with previous results, quantitative RT-PCR (qPCR) revealed that PAR2 transcript is expressed in the rat aorta (Figure A2). We also identified PAR2 expression in adult rat heart as well as isolated adult rat cardiomyocytes (Figure A2). The expression levels of PAR2 in heart and cardiomyocytes were comparable, suggesting that cardiomyocytes may be the major cell type in the heart to express PAR2.

Figure A2. PAR2 is expressed in rat aorta, heart and isolated cardiomyocytes. Quantitative RT-PCR (qPCR) analysis of extracted RNA of adult rat aorta, heart and cardiomyocytes show the expression of this receptor by aorta (possibly endothelial cells), Heart (possibly cardiomyocytes) and cardiac muscle cells (cardiomyocytes). Data represent the standard error of the mean of 4-9 independent experiments. Three technical replicates were included across each of the 4-9 biological replicates.

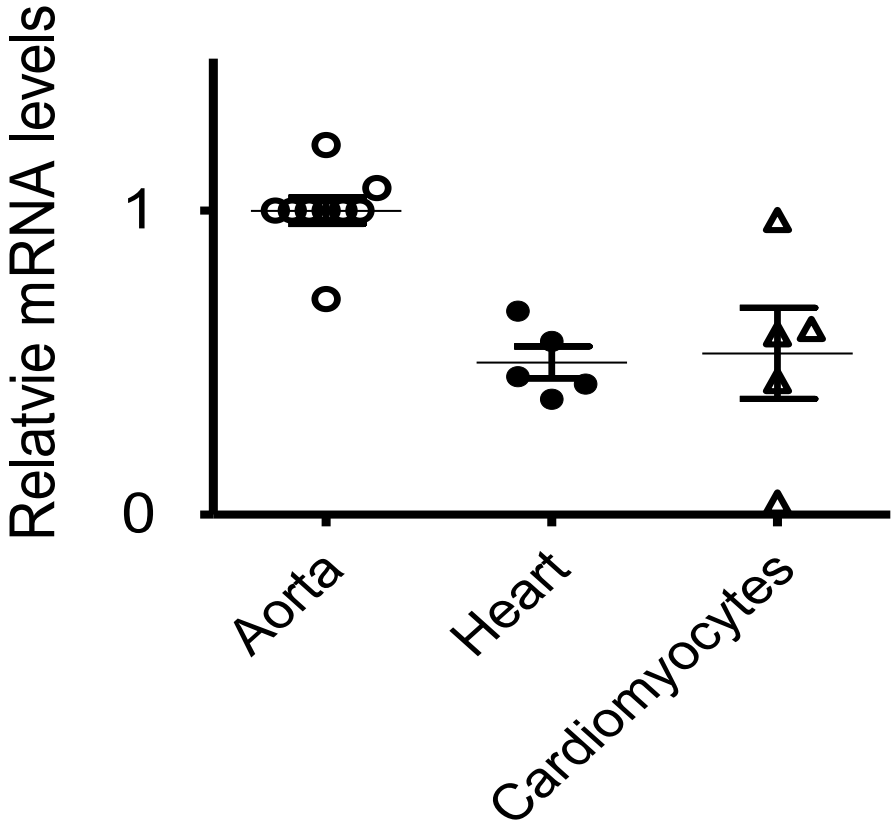
Relatvie mRNA levels
1
0
Aorta
Heart
Cardiomyocytes

A3.2. PAR-2 activation decreases the level of p-AMPK.

In order to determine the downstream pathway of this receptor and investigate the impact of PAR-2 on cell metabolism, we employed PAR-2 activator (2fli) to find the effect of this receptor on AMPK harbouring the main role in cell metabolism. Interestingly the results revealed that activation of PAR-2 negatively affects on active form of AMPK (pAMPK) (Figure A3). We confirmed these results by using the PAR-2 antagonist (GB83). Inactivation of PAR-2 by GB83 corresponded with an increase expression of pAMPK (active form of this molecule) (Figure A4). Therefore, AMPK is a potential downstream target of PAR-2. Thus, it may be possible to manipulate AMPK-regulated ATP production in cardiomyocytes according to the interaction between PAR-2 and AMPK.

Toward improving our understanding about the PAR-2 signal transduction cascade, we evaluated the effect of PAR-2 agonist and antagonist on the quantity of phosphorylation of acetyl-coA carboxylase 1. Interestingly, activation of PAR-2 by 2fLI resulted in decreased pACC (Figure A5). In line with this result, PAR-2 antagonist leads to increased pACC (Figure A6).

Figure A3. PAR2 activation decreases AMPK phosphorylation. (A) Representative immunoblot and (B) densitometric analysis of phospho-AMPK (p-AMPK) and total AMPK (T-AMPK) abundance in isolated rat cardiomyocytes treated with the PAR2 agonist 2fLI. Data represent the standard error of the mean of 5-7 independent experiments. #, $p < 0.05$ compared to untreated control.

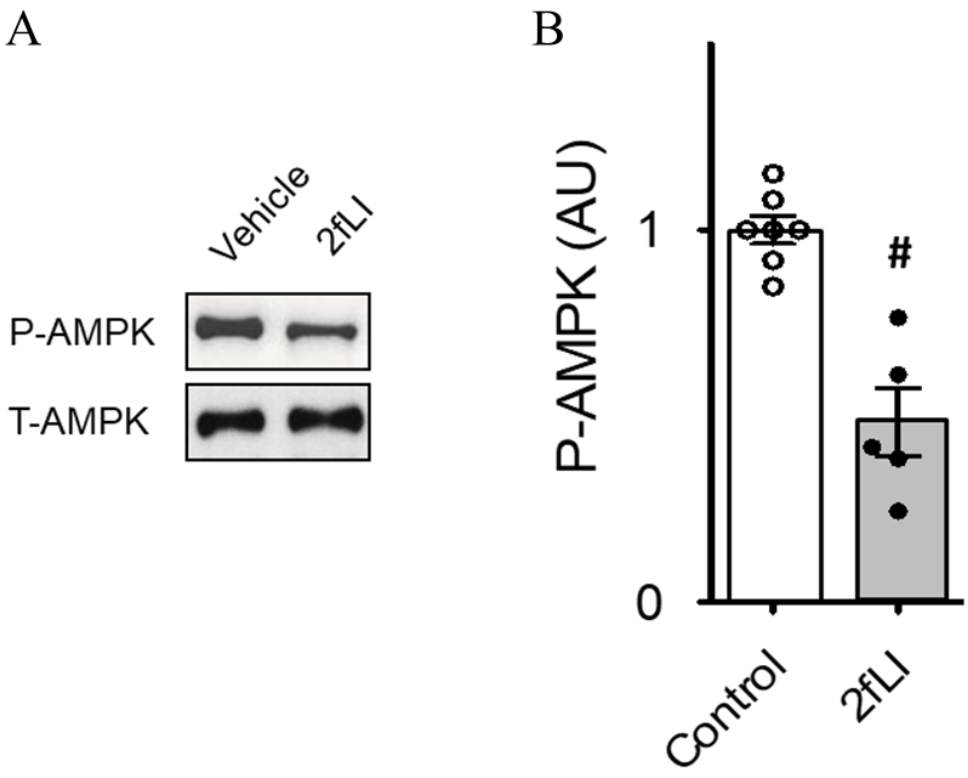
A
Vehicle
2fLI
P-AMPK
T-AMPK
B
P-AMPK (AU)
1
0
#
Control
2fLI

Figure A4. PAR2 antagonist increases phosphor-AMPK activity in isolated rat cardiomyocytes. (A) Representative immunoblot and (B) densitometric analysis of phospho-AMPK (p-AMPK) and total AMPK (T-AMPK) abundance in isolated rat cardiomyocytes treated with the PAR2 antagonist GB83. Data represent the standard error of the mean of 3 independent experiments. $p < 0.0001$ compared to untreated control.

A

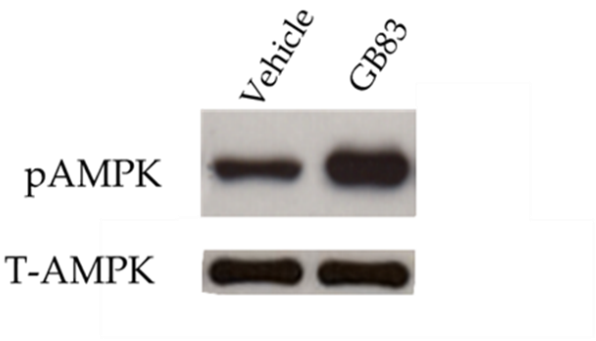
Vehicle
GB83
pAMPK
T-AMPK

B

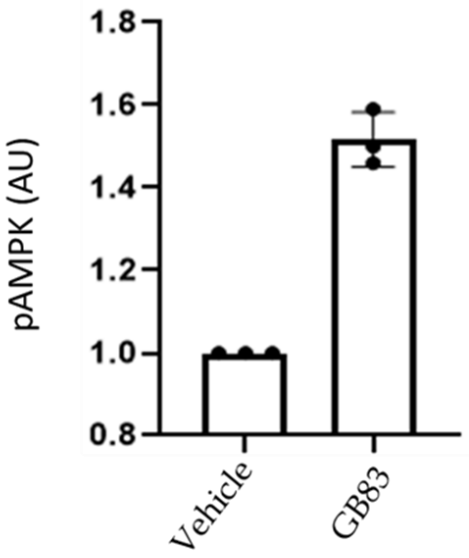
pAMPK (AU)
1.8
1.6
1.4
1.2
1.0
0.8
Vehicle
GB83

Figure A5. PAR2 receptor activation decreases pACC in adult rat cardiomyocytes. (A) Representative immunoblot and (B) densitometric analysis of phospho-ACC (pACC) abundance in isolated rat cardiomyocytes treated with the PAR2 agonist 2fLI. Data represent the standard error of the mean of 4 independent experiments.

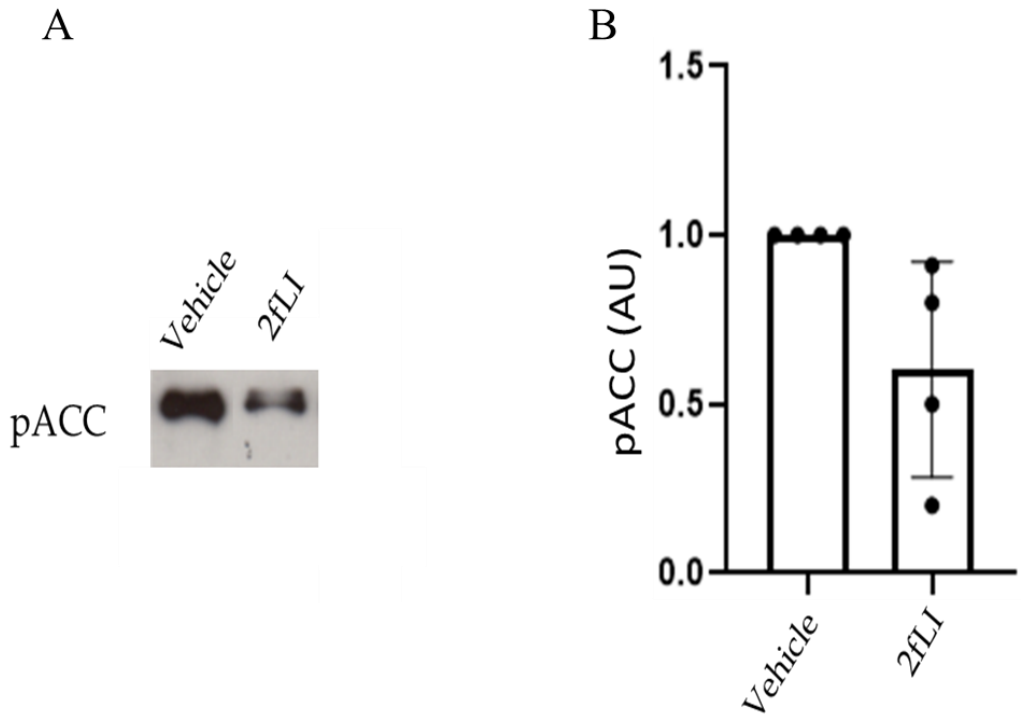
A
Vehicle
2fLI
pACC
B
1.5
1.0
0.5
0.0
pACC (AU)
Vehicle
2fLI

Figure A6. PAR2 inactivation results in increased p-ACC in adult rat cardiomyocytes. (A) Representative immunoblot and (B) densitometric analysis of phospho-ACC (pACC) abundance in isolated rat cardiomyocytes treated with the PAR2 antagonist GB83. Data represent the standard error of the mean of 3 independent experiments.

A

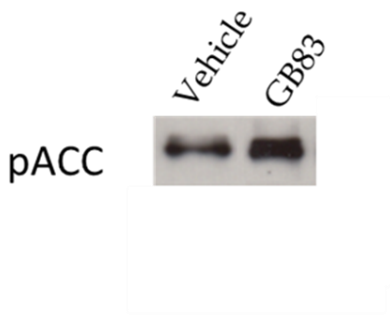

B

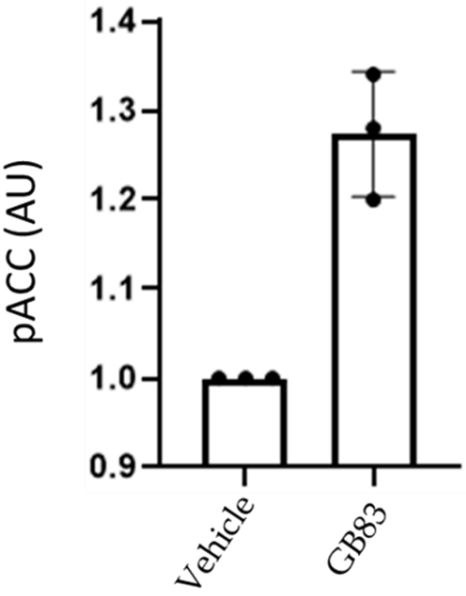

A4. Conclusions and Future Directions

A4.1. Conclusion

Myocardial infarction is a major cause of death and disability. Lifestyle choices, including smoking and obesity increase the prevalence of this disease in western cultures. Providing MI patients with intervention during the ischemic window is essential to aid recovery, as the injury becomes irreversible once reperfusion occurs. This is because reperfusion is accompanied by widespread inflammation which can irreversibly damage tissue. Supporting the heart muscle cells during this period can be a good strategy to avoid widespread cardiomyocyte cell death. We have shown here that suppressing the activity of PAR-2 leads to AMPK activation and subsequent reduction in ACC activity. Thus, it is possible that modulating PAR-2 activity during ischemia could increase the availability of ATP within a cell. Further, administering PAR2 antagonists as soon as possible after MI may help to rescue damaged cardiomyocytes and reduce heart injury. However, more investigation is required to improve our understanding about this matter.

A4.2. Future Directions

In order to determine whether PAR-2 is indeed a viable therapeutic target for ischemic-reperfusion injury, we must evaluate cardiomyocyte cell death in WT and Par2 knockout mouse hearts following MI surgery. Additionally, it would be beneficial to examine AMPK activation, glucose metabolism and fatty acid metabolism in isolated cardiomyocytes from wild type and Par2 knockout mice.

A5. References

1- Turer AT, Hill JA. Pathogenesis of myocardial ischemia-reperfusion injury and rationale for therapy. *Am J Cardiol*. 2010;106(3):360-368. doi:10.1016/j.amjcard.2010.03.032.

2. Rauch U, Osende JI, Fuster V, Badimon JJ, Fayad Z, Chesebro JH. Thrombus formation on atherosclerotic plaques: pathogenesis and clinical consequences. *Ann Intern Med*. 2001;134(3):224-238. doi:10.7326/0003-4819-134-3-200102060-00014

3- Mihaylova MM, Shaw RJ. The AMPK signalling pathway coordinates cell growth, autophagy and metabolism. *Nat Cell Biol*. 2011;13(9):1016-1023. doi:10.1038/ncb2329.

4- Antoniak S, Rojas M, Spring D, et al. Protease-activated receptor 2 deficiency reduces cardiac ischemia/reperfusion injury. *Arterioscler Thromb Vasc Biol.* 2010;30(11):2136-2142. doi:10.1161/ATVBAHA.110.213280.

5- Russell RR 3rd, Li J, Coven DL, et al. AMP-activated protein kinase mediates ischemic glucose uptake and prevents postischemic cardiac dysfunction, apoptosis, and injury. *J Clin Invest.* 2004;114(4):495-503. doi:10.1172/JCI19297.

6- Louch WE, Sheehan KA, Wolska BM. Methods in cardiomyocyte isolation, culture, and gene transfer. *J Mol Cell Cardiol*. 2011;51(3):288-298. doi:10.1016/j.yjmcc.2011.06.012

7- Egorova MV, Afanas'ev SA, Popov SV. A simple method for isolation of cardiomyocytes from adult rat heart. *Bull Exp Biol Med*. 2005;140(3):370-3. doi: 10.1007/s10517-005-0492-y.

8- Petersen A, Kutsche HS, Nippert F, Schreckenberg R, Schulz R, Schlüter KD. Induction of Proteasome Subunit Low Molecular Weight Protein (LMP)-2 Is Required to Induce Active Remodeling in Adult Rat Ventricular Cardiomyocytes. *Med Sci* (Basel). 2020;8(2):21. doi:10.3390/medsci8020021

9 -Kagota S, Maruyama K, McGuire JJ. Characterization and Functions of Protease-Activated Receptor 2 in Obesity, Diabetes, and Metabolic Syndrome: A Systematic Review. *Biomed Res Int*. 2016;2016:3130496. doi:10.1155/2016/3130496

10 -Suen JY, Barry GD, Lohman RJ, et al. Modulating human proteinase activated receptor 2 with a novel antagonist (GB88) and agonist (GB110). *Br J Pharmacol*. 2012;165(5):1413-1423. doi:10.1111/j.1476-5381.2011.01610.x

11- Yau MK, Suen JY, Xu W, et al. Potent Small Agonists of Protease Activated Receptor 2. *ACS Med Chem Lett*. 2015;7(1):105-110. doi:10.1021/acsmedchemlett.5b00429.

12- Yau MK, Liu L, Suen JY, et al. PAR2 Modulators Derived from GB88. *ACS Med Chem Lett.* 2016;7(12):1179-1184. doi:10.1021/acsmedchemlett.6b00306.

13- Gieseler F, Ungefroren H, Settmacher U, Hollenberg MD, Kaufmann R. Proteinase-activated receptors (PARs) - focus on receptor-receptor-interactions and their physiological and pathophysiological impact. *Cell Commun Signal*. 2013;11:86. doi:10.1186/1478-811X-11-86.

14- Kahn ML, Hammes SR, Botka C, Coughlin SR. Gene and locus structure and chromosomal localization of the protease-activated receptor gene family. *J Biol Chem*. 1998;273(36):23290-23296. doi:10.1074/jbc.273.36.23290.

15- Soh UJ, Dores MR, Chen B, Trejo J. Signal transduction by protease-activated receptors. *Br J Pharmacol*. 2010;160(2):191-203. doi:10.1111/j.1476-5381.2010.00705.x

16- Hollenberg MD, Renaux B, Hyun E, et al. Derivatized 2-furoyl-LIGRLO-amide, a versatile and selective probe for proteinase-activated receptor 2: binding and visualization. *J Pharmacol Exp Ther.* 2008;326(2):453-62. doi: 10.1124/jpet.108.136432.

17- Suen JY, Barry GD, Lohman RJ, et al. Modulating human proteinase activated receptor 2 with a novel antagonist (GB88) and agonist (GB110). *Br J Pharmacol.* 2012;165(5):1413-1423. doi:10.1111/j.1476-5381.2011.01610.x.

18- Gowans GJ, Hawley SA, Ross FA, Hardie DG. AMP is a true physiological regulator of AMP-activated protein kinase by both allosteric activation and enhancing net phosphorylation. *Cell Metab*. 2013;18(4):556-566. doi:10.1016/j.cmet.2013.08.019.

19- Voss M, Paterson J, Kelsall IR, Martin-Granados C, Hastie CJ, Peggie MW et al. Ppm1E is an in cellulo AMP-activated protein kinase phosphatase. *Cell Signal*. 2011; 23: 114–124. doi:10.1016/j.cellsig.2010.08.010.

20- NR Davies SP, Helps, Cohen PT, Hardie DG. 5′-AMP inhibits dephosphorylation, as well as promoting phosphorylation, of the AMP-activated protein kinase. Studies using bacterially expressed human protein phosphatase-2C alpha and native bovine protein phosphatase-2AC. *FEBS Lett.* 1995; 377: 421–425. doi:10.1016/0014-5793(95)01368-7.

21- Carling D, Clarke PR, Zammit VA, Hardie DG. Purification and characterization of the AMP-activated protein kinase. Copurification of acetyl-CoA carboxylase kinase and 3-hydroxy-3-methylglutaryl-CoA reductase kinase activities. *Eur J Biochem* 1989; 186: 129–136. doi:10.1111/j.1432-1033.1989.tb15186.x.

22- Kraegen EW, Saha AK, Preston E, et al. Increased malonyl-CoA and diacylglycerol content and reduced AMPK activity accompany insulin resistance induced by glucose infusion in muscle and liver of rats. *Am J Physiol Endocrinol Metab* 2006; 290: E471–E479. doi:10.1152/ajpendo.00316.2005.

9. Appendix B. Human Ethics approval

Subject **HREB - Approval of Ethics Renewal 510179**
From <administrator@hrea.ca>
To Esseltine Jessica(Principal Investigator) <jesseltine@mun.ca>
Cc <administrator@hrea.ca>
Date 2020-10-06 08:59

roundcube
open source webmail software

Researcher Portal File #: 20191777

Dear Dr. Jessica Esseltine:

This e-mail serves as notification that your ethics renewal for study HREB # 2018.210 – Connexins and Pannexins in Stem Cell Pluripotency and Cell Fate Decisions – has been **approved**. Please log in to the Researcher Portal to view the approved event.

Ethics approval for this project has been granted for a period of twelve months effective from 13 Nov 2020 to 13 Nov 2021.

Please note, it is the responsibility of the Principal Investigator (PI) to ensure that the Ethics Renewal form is submitted prior to the renewal date each year. Though the Research Ethics Office makes every effort to remind the PI of this responsibility, the PI may not receive a reminder. The Ethics Renewal form can be found on the Researcher Portal as an "Event".

Thank you,

Research Ethics Office

(e) info@hrea.ca
(t) 709-777-6974
(f) 709-777-8776
(w) www.hrea.ca
Office Hours: 8:30 a.m. – 4:30 p.m. (NL TIME) Monday-Friday